Available online at www.sciencedirect.com
ScienceDirect
Comput. Methods Appl. Mech. Engrg. 417 (2023) 116341
Computer methods in applied mechanics and engineering
www.elsevier.com/locate/cma

A review of VMS a posteriori error estimation with emphasis in fluid mechanics

Guillermo Hauke*, Diego Irisarri

Fluid Mechanics Department – Instituto de Investigacion en Ingenieria de Aragon (I3A), Escuela de Ingeniería y Arquitectura, Área de Mecánica de Fluidos, Universidad de Zaragoza, C/María de Luna 3, 50018 Zaragoza, Spain

Available online 19 August 2023

Abstract

This article outlines the research on the application of the variational multiscale theory (VMS) to a posteriori error estimation. VMS theory was initially developed by Professor Hughes to evince the origins of stabilized methods. In this paper it is shown that the stabilization parameters and the stabilization terms contain true error information that can be used to obtain explicit and implicit a posteriori error estimates. The technology consists of splitting the exact solution into resolved or coarse scales (finite element solution) and unresolved or fine scales (numerical error). By feeding this splitting into the variational formulation, an exact weak form can be derived for the fine scales as a function of the resolved scales. The way of solving or approximating this equation yields different algorithms and models for error estimation. Furthermore, using the so-called fine-scale Green's function, an analytical representation of the fine scales is possible. Again, different approximations of this function give rise to various algorithms and models. This theory naturally suggests that the error can be computed by the combination of element interior and inter-element faces residuals with the corresponding error time-scales. From this standpoint, error estimators are developed for the transport equation and the Navier–Stokes equations. This technology can be further used for example to generate adapted meshes, to derive reduced order models and in verification and validation algorithms.

Keywords: A posteriori error estimation; Adaptivity; Variational multiscale method; Transport equations; Euler equations; Navier–Stokes equations

1. Introduction

Stabilized methods [1–3] have been around now for a few decades. In particular, in [4,5] Professor Hughes unveiled that the extra variational integral added to the Galerkin method amounts to incorporate the error of the numerical method into the finite element solution. These last two papers (extended to the transient case in [6]) point also out that any stabilized method can be understood as a posteriori error estimator and, conversely, any error estimator can be interpreted as a potential stabilized method. This powerful and simple idea then would close the circle quadrature since each stabilized method would possess its own a posteriori error estimator, opening a new avenue for investigation. Thus, the goal of this paper is to summarize the investigations in our group on applying the variational multiscale approach (VMS) to the development of explicit and implicit *a posteriori* error estimators in general, and to fluid transport problems in particular.

* Corresponding author.
E-mail address: ghauke@unizar.es (G. Hauke).

https://doi.org/10.1016/j.cma.2023.116341

Let us recall that *a posteriori* error estimation methods can be classified as residual based methods, recovery-based methods and auxiliary-problem-based methods [7].

1. *Residual-based methods* estimate the error of the solution directly by computing residuals, both, interior and/or inter-element or boundary residuals. Typically, they postprocess the discrete finite element solution, and so, are called *explicit* methods. Explicit residual-based error estimators were proposed for the first time by Babuška and Rheinbolt [8], and then extended to two-dimensions in [9,10].
2. *Recovery-based methods* use up superconvergent properties of the solutions and were first proposed by [11,12]. They can be used at the element level or using patches of elements [13,14]. A general framework for the analysis of the above methods can be found in [15]. For applications to aerodynamics see [16,17] and for a recent contribution, [18].
3. *Auxiliary-problem-based methods*. In this technique, new partial differential equations are solved either at the element level, in subdomains or in the whole domain. Since estimating the error requires solving a new problem, they are also called *implicit* error estimators. Pioneering work was started by [19–22]. Important contributions are those in [23–26], for instance.

A posteriori error estimation is in general a vast field, that was initiated for elliptic problems by Babuška and Rheinbolt [19], and then followed by Zienkiewicz and Zhu [11,12], Eriksson and Johnson [27], Ainsworth and Oden [28], among others. Stewart and Hughes also made contributions in [29,30]. The above ideas were then applied to hyperbolic and fluid mechanics problems, for instance by Oden et al. [31,32], Johnson and coworkers [33–35], Strouboulis and Oden [36], and Verfürth [37]. Developing strict bounds for linear-functionals of the solution is another promising approach to error control (see [38–42]).

For the Stokes equations, we remark the work of Verfürth [43], Kay and Silvester [44], Bank and Welfert [45] and, more recently, Larsson et al. [46] that propose implicit estimators which imply the solution of local problems at the element level. The error is measured in energy-like norms. On the other hand, Ainsworth and Oden [47] and Nobile [48], develop implicit error estimators which provide the lower and upper bounds of the error. In [49], Russo proposes an explicit error estimator for the MINI-element employing bubble functions. Song et al. [50] take advantage of VMS to develop an error estimator oriented towards generating adapted meshes.

As regards to the Navier–Stokes equations, Johnson and coworkers established residual-based error estimates in various norms and their application to incompressible flow can be found in [51]. Ainsworth and Oden in [47,52] established an error estimation measured in a energy-like norm which is bounded. Berrone presented a residual-based approach in [53,54], where the influence of the Reynolds number is made explicit and the error estimate is used to adapt the mesh.

For a more elaborate review on the topic, the reader can consult [7,55–57]. Furthermore, [58,59] review and compare the performance of the most successful *a posteriori* error estimators when applied to fluid mechanics problems. And despite of the breadth of the subject, their conclusions are not optimistic, since all authors conclude that for fluid transport, present techniques are far from satisfactory. Simple algorithms are *non-robust*, that is, the ratio of predicted to true error changes dramatically with the diffusion coefficient (see [60,61]). Some solutions exist but require solving additional partial differential equations, which can turn computationally expensive.

Beyond the ideas outlined in this paper, VMS a posteriori error estimation has found application in other areas, such as reduced-order models [62,63], uncertainty quantification [64,65], isogeometric analysis [66,67] and convergence and accuracy enhancement of finite element solutions [68].

2. The transport equation

The transport equation is a simple linear model of fluid motion, ideal to illustrate the main ideas on a posteriori error estimation driven by the variational multiscale theory (VMS).

2.1. Preliminaries

Consider a spatial domain Ω with boundary Γ, which is partitioned into two non-overlapping zones Γ_g and Γ_h. Let $\boldsymbol{x}$ and $\boldsymbol{y}$ be two points in $\overline{\Omega}$. The *strong form* of the boundary-value problem consists of finding $u : \Omega \to \mathbb{R}$

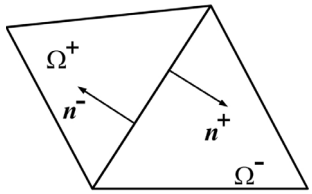

Fig. 1. Notation for the jump across element interfaces.

such that for the given essential boundary condition $\mathrm{g} : \Gamma_g \to \mathbb{R}$, the natural boundary condition $h : \Gamma_h \to \mathbb{R}$, and forcing function $f : \Omega \to \mathbb{R}$, the following equations are satisfied

$$\left\{\begin{array}{rcll} \mathcal{L}u & = f & \text{in} & \Omega \\ u & = \mathrm{g} & \text{on} & \Gamma_g \\ \mathcal{B}u & = h & \text{on} & \Gamma_h \end{array}\right. \tag{1}$$

where $\mathcal{L}$ is in principle a second-order differential operator and $\mathcal{B}$, an operator defined later, acting on the boundary.

Next, let us define the *weak form*. Given the functional solution space $\mathcal{S} \subset H^1(\Omega)$ and weighting space $\mathcal{V} \subset H^1(\Omega)$, with $H^1(\Omega)$ the Sobolev space of order one [69],

$$\begin{array}{l} \mathcal{S} = \{u \in H^1(\Omega) \mid u = g \quad \text{on} \quad \Gamma_g\} \\ \mathcal{V} = \{v \in H^1(\Omega) \mid v = 0 \quad \text{on} \quad \Gamma_g\} \end{array} \tag{2}$$

the variational formulation for the above boundary-value problem consists of finding $u \in \mathcal{S}$ such that:

$$a(w, u) = (w, f) + (w, h)_{\Gamma_h} \qquad \forall w \in \mathcal{V} \tag{3}$$

where $(\cdot, \cdot)$ is the $L_2(\Omega)$ inner product, $(\cdot, \cdot)_\omega$ is the $L_2(\omega)$ inner product in the domain ω, and $a(\cdot, \cdot)$ is a bilinear form satisfying

$$a(w, u) = (w, \mathcal{L}u) + (w, \mathcal{B}u)_{\Gamma_h} \tag{4}$$

for all sufficiently smooth functions $w \in \mathcal{V}$ and $u \in \mathcal{S}$. Likewise, $a(\cdot, \cdot)_\omega$ is the bilinear operator with the integral extended over the domain ω.

In the case of finite element methods, the domain Ω is discretized into n_{el} non-overlapping elements with domain Ω^e and boundary Γ^e ($e = 1, 2, \ldots, n_{\text{el}}$). The functions then may be discontinuous across the inter-element boundaries. Let us denote the union of element interiors as $\widetilde{\Omega}$, where $\widetilde{\Omega} = \bigcup_{e=1}^{n_{\text{el}}} \Omega^e$ and the union of element boundaries minus Γ as $\widetilde{\Gamma}$, with $\widetilde{\Gamma} = \bigcup_{e=1}^{n_{\text{el}}} \Gamma^e \setminus \Gamma$ also referred to as the element interfaces or inter-element boundaries. Furthermore, let $[\![\cdot]\!]$ denote the jump operator of a function across an inter-element boundary. Following the notation of Fig. 1, where the respective outward unit normals to elements Ω^+ and Ω^- are $\boldsymbol{n}^+$ and $\boldsymbol{n}^-$, the jump of $\boldsymbol{v} \cdot \boldsymbol{n}$ is defined as [69]

$$[\![\boldsymbol{v} \cdot \boldsymbol{n}]\!] = \boldsymbol{n}^+ \cdot \boldsymbol{v}^+ + \boldsymbol{n}^- \cdot \boldsymbol{v}^- \tag{5}$$

2.2. The variational multiscale approach to error estimation

Professor Hughes evinced the origin of the variational multiscale theory in the seminal works [4,5] by applying the concept of scale splitting to the solution u and weighting functions w,

$$\begin{array}{llll} u & = \bar{u} + u' & \bar{u} \in \bar{\mathcal{S}} & u' \in \mathcal{S}' \\ w & = \bar{w} + w' & \bar{w} \in \bar{\mathcal{V}} & w' \in \mathcal{V}' \end{array} \tag{6}$$

where $\bar{\mathcal{S}}$, $\bar{\mathcal{V}}$ and $\mathcal{S}'$, $\mathcal{V}'$ denote the respective resolved and unresolved scales finite element spaces, satisfying $\mathcal{S}' = \mathcal{S} \setminus \bar{\mathcal{S}}$ and $\mathcal{V}' = \mathcal{V} \setminus \bar{\mathcal{V}}$. For our purposes, u represents the *exact solution*; $\bar{u}$, the *resolved scales* or finite element solution; and u', the *unresolved scales, subgrid scales* or *error*.

The above decomposition can be substituted in the variational formulation (3). Because of its bilinearity, the weak form is equivalent to these two subproblems,

$$a(\bar{w}, \bar{u}) = -a(\bar{w}, u') + (\bar{w}, f) + (\bar{w}, h)_{\Gamma_h} \tag{7a}$$

$$a(w', u') = -a(w', \bar{u}) + (w', f) + (w', h)_{\Gamma_h} \tag{7b}$$

the first one for the resolved scales $\bar{u}$ and the second one for the unresolved scales u'.

For smooth functions within the element interiors but rough across the inter-element boundaries, such as finite element functions, integration by parts of $a(w', \bar{u})$ leads to

$$\begin{aligned} a(w', \bar{u}) &= \sum_{e=1}^{n_{\text{el}}} a(w', \bar{u})_{(\Omega^e)} \\ &= \sum_{e=1}^{n_{\text{el}}} \left\{ (w', \mathcal{L}\bar{u})_{(\Omega^e)} + (w', \mathcal{B}\bar{u})_{\Gamma^e} \right\} \\ &= (w', \mathcal{L}\bar{u})_{\widetilde{\Omega}} + (w', [\![\mathcal{B}\bar{u}]\!])_{\widetilde{\Gamma}} + (w', \mathcal{B}\bar{u})_{\Gamma_h} \end{aligned} \tag{8}$$

Consequently, the fine-scale subproblem (7b) can be written as

$$\begin{aligned} a(w', u') &= -(w', \mathcal{L}\bar{u})_{\widetilde{\Omega}} - (w', [\![\mathcal{B}\bar{u}]\!])_{\widetilde{\Gamma}} - (w, \mathcal{B}\bar{u})_{\Gamma_h} \\ &\quad + (w', f) + (w', h)_{\Gamma_h} \\ &= -(w', \mathcal{L}\bar{u} - f)_{\widetilde{\Omega}} - (w', [\![\mathcal{B}\bar{u}]\!])_{\widetilde{\Gamma}} - (w', \mathcal{B}\bar{u} - h)_{\Gamma_h} \end{aligned} \tag{9}$$

Finally, the fine-scale problem (9) can be solved analytically using the Green's function of the fine-scale problem, $g'(\boldsymbol{x}, \boldsymbol{y})$, so the error can be exactly computed as

$$\boxed{\begin{aligned} u'(\boldsymbol{x}) = \quad & -\int_{\widetilde{\Omega}_y} g'(\boldsymbol{x}, \boldsymbol{y})\, (\mathcal{L}\bar{u} - f)(\boldsymbol{y})\, \mathrm{d}\Omega_y \\ & -\int_{\widetilde{\Gamma}_y} g'(\boldsymbol{x}, \boldsymbol{y})\, ([\![\mathcal{B}\bar{u}]\!])(\boldsymbol{y})\, \mathrm{d}\Gamma_y \\ & -\int_{\Gamma_{hy}} g'(\boldsymbol{x}, \boldsymbol{y})\, (\mathcal{B}\bar{u} - h)(\boldsymbol{y})\, \mathrm{d}\Gamma_y \end{aligned}} \tag{10}$$

The fine-scale Green's function is the projection of the classic Green's function into the unresolved-scales space. This concept was introduced in [4,5] and was further investigated and formally defined in [70]. The interested reader is referred to the above publications for a more detailed information.

Remarks.

1. The same result can be expressed via the Green's function of the adjoint fine-scale problem g'^* through the identity $g'(\boldsymbol{x}, \boldsymbol{y}) = g'^*(\boldsymbol{y}, \boldsymbol{x})$.
2. Note that the integral is non-local and, therefore, the effect of the error is, in principle, non-local. For instance, the error at a singularity can influence the precision at distant places. This is called the *pollution* effect [7]. For certain problems and computational methods, such as stabilized methods, the pollution effect is mostly locally restrained.
3. The error estimator is residual-based. The contemplated residuals include:
   i. Element interior residuals, $\mathcal{L}\bar{u} - f$ in $\widetilde{\Omega}$.
   ii. Inter-element residuals, $[\![\mathcal{B}\bar{u}]\!]$ on $\widetilde{\Gamma}$.
   iii. Natural boundary condition residual, $\mathcal{B}\bar{u} - h$ on Γ_h.
4. Other sources of errors, such as Dirichlet boundary condition approximations or boundary approximation, are not considered here.
5. The fine-scale Green's function $g'(\boldsymbol{x}, \boldsymbol{y})$ is the distribution that characterizes the behavior of the numerical error, and emanates from the proper projection of the global Green's function. Therefore, it depends on the operator (with the corresponding geometry and boundary conditions), on the finite element space and on the method (or projector). Furthermore, $\mathcal{S}'$ is the kernel of the projector that defines the method and can also be viewed as the quotient space $\mathcal{S}' = \mathcal{S}/\bar{\mathcal{S}}$ (see [70] for further details).
6. Even though (10) is exact for a linear problem, the calculation of the fine-scale Green's function can be more complex than that of the solution of the original problem. In order to simplify the procedure, a simpler strategy based on approximations compatible with the theory of stabilized methods is proposed.

7. Using global Green's functions to compute the pointwise error was investigated for elasticity problems in [71,72] and the link between finite elements and Green's functions in [73]. Also Estep et al. [74] use global Green's functions to study the domain of influence of the error in elliptic problems. These ideas will be revisited in the section on the nature of the finite element error, where it will be shown that the pollution error can be exactly computed as a combination of global free-space Green's functions.

2.3. A model for error estimation

The error representation (10) can be split into errors stemming from element interior residuals $u'_{\text{int}}(\boldsymbol{x})$ and element boundary residuals $u'_{\text{bnd}}(\boldsymbol{x})$ [75,76], namely

$$u'(\boldsymbol{x}) = u'_{\text{int}}(\boldsymbol{x}) + u'_{\text{bnd}}(\boldsymbol{x}) \tag{11}$$

Therefore, using the triangle inequality [75] we can write

$$\|u'(\boldsymbol{x})\| \leq \|u'_{\text{int}}(\boldsymbol{x})\| + \|u'_{\text{bnd}}(\boldsymbol{x})\| \tag{12}$$

2.3.1. Element interior error

In [70] it is shown that for certain types of variational methods, such as stabilized methods, the error distribution is *practically local*. For these methods, the fine-scale Green's function can be approximated by the *element* Green's function $g_e(\boldsymbol{x}, \boldsymbol{y})$, which is the classic Green's function defined within the domain of one element [4,5].

Therefore, following [77–79] the error due to element interiors can modeled as the smooth paradigm,

$$u'_{\text{int}}(\boldsymbol{x}) \approx \quad -\int_{\Omega^e_y} g_e(\boldsymbol{x}, \boldsymbol{y})\ (\mathcal{L}\bar{u} - f)(\boldsymbol{y})\ \mathrm{d}\Omega_y \qquad \text{on } \Omega^e \tag{13}$$

As stated earlier, (13) is exact for element-edge-exact solutions.

By Hölders inequality (see Brenner and Scott [80]) we can develop an (approximate) upper bound,

$$|u'_{\text{int}}(\boldsymbol{x})| \leq \|g_e(\boldsymbol{x}, \boldsymbol{y})\|_{L_p(\Omega^e_y)}\ \|\mathcal{L}\bar{u} - f\|_{L_q(\Omega^e)} \tag{14}$$

with $1 \leq p, q \leq \infty$, $1/p + 1/q = 1$. Taking the L_r norm,

$$\boxed{\|u'_{\text{int}}(\boldsymbol{x})\|_{L_r(\Omega^e)} \leq \Big|\Big|\ \|g_e(\boldsymbol{x}, \boldsymbol{y})\|_{L_p(\Omega^e_y)}\Big|\Big|_{L_r(\Omega^e_x)}\ \|\mathcal{L}\bar{u} - f\|_{L_q(\Omega^e)}} \tag{15}$$

Remark. This contribution is vital for error estimation in the hyperbolic limit.

2.3.2. Element boundary error

The term $u'_{\text{bnd}}(x)$ is connected to the non-smooth derivatives across the element boundaries of the finite element solution, $\bar{u}$. The inter-element boundary errors are approximated within each element as

$$u'_{\text{bnd}}(\boldsymbol{x}) \quad \approx -\int_{\Gamma^e_y} g'(\boldsymbol{x}, \boldsymbol{y})\ (\llbracket \mathcal{B}\bar{u} \rrbracket)(\boldsymbol{y})\ \mathrm{d}\Gamma_y \qquad \text{on } \Omega^e \tag{16}$$

where the jump definition has been formally extended to encompass the natural boundary condition residual,

$$\llbracket \mathcal{B}\bar{u} \rrbracket = \begin{cases} \mathcal{B}\bar{u} - h & \text{on } \Gamma^e \cap \Gamma_h \\ 0 & \text{on } \Gamma^e \cap \Gamma_g \end{cases} \tag{17}$$

Note that the inter-element boundary integral on $\widetilde{\Gamma}$ has been replaced by the boundary integral along Γ^e. Since this integral contains the jump of the flux, $\mathcal{B}\bar{u}$, it increases the non-locality by one layer of elements around Ω^e.

Again, by Hölders inequality

$$|u'_{\text{bnd}}(\boldsymbol{x})| \leq \|g'(\boldsymbol{x}, \boldsymbol{y})\|_{L_p(\Gamma^e_y)}\ \|\llbracket \mathcal{B}\bar{u} \rrbracket\|_{L_q(\Gamma^e)} \tag{18}$$

with $1 \leq p, q \leq \infty$, $1/p + 1/q = 1$ and taking the L_r norm,

$$\boxed{\|u'_{\text{bnd}}(\boldsymbol{x})\|_{L_r(\Omega^e)} \leq \Big|\Big|\ \|g'(\boldsymbol{x}, \boldsymbol{y})\|_{L_p(\Gamma^e_y)}\Big|\Big|_{L_r(\Omega^e_x)}\ \|\llbracket \mathcal{B}\bar{u} \rrbracket\|_{L_q(\Gamma^e)}} \tag{19}$$

Remarks.

1. This contribution is vital for error estimation in the diffusive limit.
2. Larson and Målqvist [81] state that most of the error lays within one layer of elements around Ω^e, confirming the above approximation.
3. Still, g' needs to be related to a simpler function, such as g_e. This is done in the next subsection.

2.3.3. Norms based on the L_∞ norm of the residual

Because the Green's function may not be very smooth in multidimensional applications, the choice $p = 1$ and $q = \infty$ stands out. Then, typical choices for r are $r = 1$ or $r = 2$. In this case, if $g_e(\boldsymbol{x}, \boldsymbol{y})$ does not change sign in Ω^e,

$$\left|\left| \|g_e(\boldsymbol{x}, \boldsymbol{y})\|_{L_1(\Omega^e_{\boldsymbol{y}})} \right|\right|_{L_r(\Omega^e_{\boldsymbol{x}})} = \|b^e_0(\boldsymbol{x})\|_{L_r(\Omega^e_{\boldsymbol{x}})} \tag{20}$$

where the function $b^e_0(\boldsymbol{x})$ is a *residual-free bubble* [82–84]. Then, the error time scales can be defined as norms or averages of residual-free bubbles [78],

$$\tau^e_{L_1} = \frac{1}{\text{meas}(\Omega^e)} \|b^e_0(\boldsymbol{x})\|_{L_1(\Omega^e)} \qquad \tau^e_{L_2} = \frac{1}{\text{meas}(\Omega^e)^{1/2}} \|b^e_0(\boldsymbol{x})\|_{L_2(\Omega^e)} \tag{21}$$

Remarks.

1. The above equations show the relation between element Green's functions, residual-free bubbles and error time-scales.
2. Note that whereas the norms of the element Green's function depend on the dimensionality of the problem, the error time scales do not. Time scales have the advantage that allow comparison between the various norm choices and the flow time scale.

Now, an approximate analysis [75] shows that the norm of the fine-scale Green's function on Γ^e can be approximately linked to the norm of the element Green's function in the domain Ω^e by

$$\left|\left| \|g'(\boldsymbol{x}, \boldsymbol{y})\|_{L_1(\Gamma^e_{\boldsymbol{y}})} \right|\right|_{L_r(\Omega^e_{\boldsymbol{x}})} \approx \frac{1}{2} \frac{\text{meas}(\Gamma^e)}{\text{meas}(\Omega^e)} \left|\left| \|g_e(\boldsymbol{x}, \boldsymbol{y})\|_{L_1(\Omega^e_{\boldsymbol{y}})} \right|\right|_{L_r(\Omega^e_{\boldsymbol{x}})} \tag{22}$$

2.3.4. Summary of the model

Gathering all the contributions of the model, the a posteriori error estimator is defined as

$$\begin{aligned} \|u'(x)\|_{L_r(\Omega^e)} \quad &\leq \text{meas}(\Omega^e)^{1/r} \ \tau_{L_r} \\ &\times \left(\|\mathcal{L}\bar{u} - f\|_{L_\infty(\Omega^e)} + \tfrac{1}{2} \frac{\text{meas}(\Gamma^e)}{\text{meas}(\Omega^e)} \|[\![\mathcal{B}\bar{u}]\!]\|_{L_\infty(\Gamma^e)} \right) \\ &\qquad \text{on } \Omega^e \end{aligned} \tag{23}$$

Remarks.

1. This is an explicit a-posteriori error estimator.
2. It is very similar to the estimator proposed by [37] and its extensions, with the advantage that it is constant-free, that is, the method gives the error constant.
3. The error constants are dimensionally correct.
4. In principle, the theory allows the error estimate in the norm of choice, assuming that the corresponding norm of the element Green's function exists.
5. In [85], the stabilizing parameter is tuned to predict the error norm exactly in the one-dimensional case. Here, this parameter is predicted by the theory and there is no need to solve local problems. The present method is also exact for one-dimensional solutions which are nodally exact.
6. Russo shows in [86] a relation between residual-based error estimators and bubble functions for elliptic problems.
7. Masud et al. in [87] consider using interior shape functions that are nonzero along the element edges for the diffusion–reaction equation.

2.4. Relation to the flow time-scale parameter

Selecting above $p = 1$, $q = \infty$, $r = 1$, then,

$$\|u'(\boldsymbol{x})\|_{L_1(\Omega^e)} \leq \|g_e(\boldsymbol{x}, \boldsymbol{y})\|_{L_1(\Omega^e_x \times \Omega^e_y)} \; \|\mathcal{L}\bar{u} - f\|_{L_\infty(\Omega^e)} \tag{24}$$

But for $g_e \geq 0$, the definition of τ^e_{flow} [4] is precisely

$$\tau^e_{\text{flow}} = \frac{1}{\text{meas}(\Omega)^e} \; \|g_e(\boldsymbol{x}, \boldsymbol{y})\|_{L_1(\Omega^e_x \times \Omega^e_y)} \tag{25}$$

Therefore, the flow time-scale parameter τ^e_{flow} gives an upper bound in the L_1 norm of the solution error as a function of the L_∞ norm of the residual. Thus,

$$\boxed{\|u'(\boldsymbol{x})\|_{L_1(\Omega^e)} \leq \tau^e_{\text{flow}} \; \text{meas}(\Omega)^e \; \|\mathcal{L}\bar{u} - f\|_{L_\infty(\Omega^e)}} \tag{26}$$

Remarks.

1. For piecewise constant residuals and nodally exact solutions, the above expression holds with the equal sign.
2. All the above results can be extended to more general cases, such as higher-order elements [88], piecewise linear residuals [79] and other norms [78].
3. For parabolic problems, the so-called stability factors in [89] play here the role of error time-scales.

2.5. Example: error time scales for the one-dimensional case

In the case of nodally exact finite element solutions, the fine-scale Green's function is precisely equal to the element Green's function $g_e(x, y)$ [70,77], which can be obtained as the solution of the following problem

$$\begin{cases} \mathcal{L}g_e &= \delta_y \quad \text{in} \quad \Omega^e \\ g_e &= 0 \quad \text{on} \quad \Gamma^e \end{cases}$$

where $\delta_y(x) = \delta(x - y)$ is the Dirac's delta function.

Therefore, in this context the error in each element Ω^e depends only on residuals inside the element. That is, the error estimator becomes

$$u'(x) = -\int_{(\Omega^e)} g_e(x, y) \; (\mathcal{L}\bar{u} - f)(y) \; \mathrm{d}\Omega_y \qquad \text{on } \Omega^e \tag{27}$$

If the residual is constant inside the element, i.e., $(\mathcal{L}\bar{u} - f) \in \mathcal{P}_0$, Eq. (27) reveals that

$$\begin{aligned} u'(x)|_{(\Omega^e)} &= -\int_{\Omega_e} g_e(x, y)(\mathcal{L}\bar{u} - f)(y) \; \mathrm{d}\Omega_y \\ &= -(\mathcal{L}\bar{u} - f) \int_{\Omega_e} g_e(x, y) \; \mathrm{d}\Omega_y \\ &= -(\mathcal{L}\bar{u} - f) \; b^e_0(x) \end{aligned} \tag{28}$$

where $b^e_0(x) = \int_{\Omega_e} g_e(x, y) \; \mathrm{d}\Omega_y$ is a *residual-free* bubble function [77,82–84], also solution of the problem

$$\begin{cases} \mathcal{L}b^e_0 &= 1 \quad \text{in} \quad \Omega^e \\ b^e_0 &= 0 \quad \text{on} \quad \Gamma^e \end{cases} \tag{29}$$

In relation to the bubble function, again we obtain the *error scale*, $\tau^e_{L_r}$, as

$$\boxed{\tau^e_{L_r} = \frac{1}{\text{meas}(\Omega^e)^{1/r}} \; \|b^e_0(x)\|_{L_r(\Omega^e)}} \tag{30}$$

For the transport equation, this parameter has dimensions of time and it becomes an *error time-scale*, similarly to the *flow* stabilization parameter employed to stabilize the Galerkin method in stabilized methods [4].

The above concepts on a posteriori error estimation are applied to one-dimensional advection–diffusion–reaction problems, where $\mathcal{L}u = au_{,x} - \kappa u_{,xx} - su$, with a the fluid velocity, κ the diffusivity and s a source parameter [78,79].

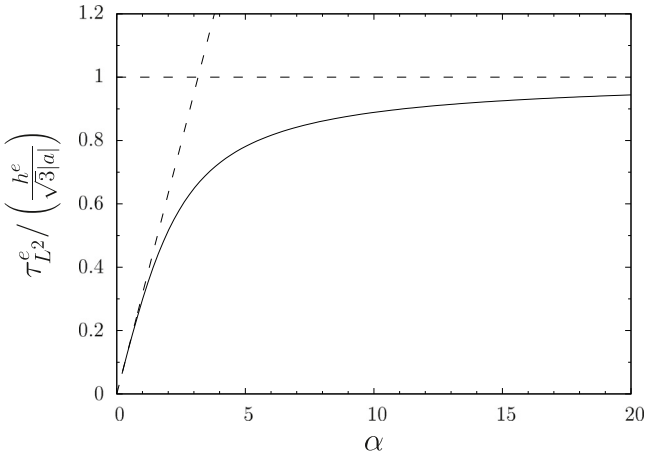

Fig. 2. One-dimensional advection–diffusion problem. Exact and asymptotic dimensionless error time-scale $\tau^e_{L_2}$ as a function of the element Peclet number α.

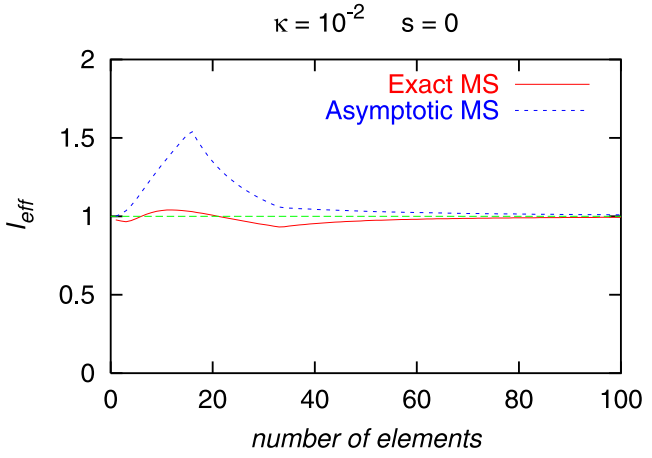

Fig. 3. Global effectivity index for one dimensional advection–diffusion. "Exact MS" shows the results employing the exact expression for the error time-scale and "Asymptotic MS", the results using the asymptotic approximation depicted in Fig. 2.

Fig. 2 shows the error time-scale $\tau^e_{L_2}$ as a function of the element Peclet number $\alpha = |a|h^e/(2\kappa)$, where h^e is the element length. As can be seen, the behavior of the error time-scale is very similar to that of the stabilization parameter τ^e_{flow}.

The technology is successful for element Peclet numbers ranging from the diffusion dominated regime till the advection dominated regime. This is illustrated in Fig. 3, where the global effectivity index is shown as a function of the number of elements for an advection-dominated example. As can be appreciated, the predicted error is exact. The finite element solution is computed with the SGS stabilized method [90–92].

2.6. Error time-scales for the bilinear quad

In this section, we calculate the 2D error time scales for the bilinear quad. For the linear triangle, see [75].

Hyperbolic limit. In the hyperbolic limit, the residual-free-bubble is the solution of the problem

$$\begin{cases} |\boldsymbol{a}|\nabla_a b_0^e = 1 & \text{in} \quad \Omega^e \\ b_0^e = 0 & \text{on} \quad \Gamma^e_{\text{in}} \end{cases}$$

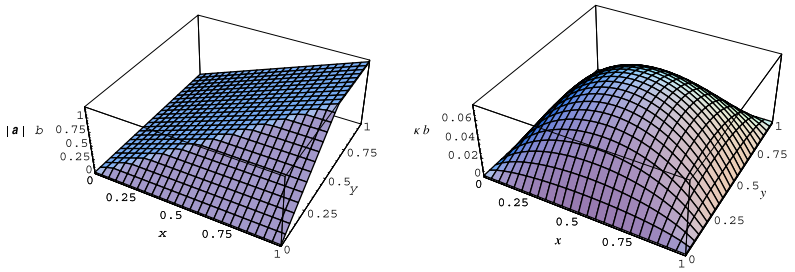

(a) (b)

Fig. 4. Bubble function $b_0^e(x, y)$ for the rectangular element in the (a) hyperbolic limit for a velocity of $\boldsymbol{a} = (\sin 30, \cos 30)$ (b) diffusive limit.

where $\boldsymbol{a}$ is the velocity; ∇_a, the derivative in the direction of $\boldsymbol{a}$ and Γ_{in}^e denotes the inflow portion of the boundary, where $\boldsymbol{a} \cdot \boldsymbol{n} < 0$. The solution can be expressed as (see Fig. 4)

$$b_0^e(\boldsymbol{x}) = \begin{cases} \dfrac{y}{|\boldsymbol{a}| \sin\theta} & y < \dfrac{a_y}{a_x} x \\ \dfrac{x}{|\boldsymbol{a}| \cos\theta} & y > \dfrac{a_y}{a_x} x \end{cases} \tag{31}$$

For a rectangular element of sides h_x and h_y, the norms of $b_0^e(\boldsymbol{x})$ yield the corresponding error time scales,

$$\tau_{L_1}^e = \frac{\|b_0\|_{L_1(\Omega^e)}}{\text{meas}(\Omega^e)} = \frac{h_{\text{flow}}}{2|\boldsymbol{a}|}\left(1 - \frac{1}{3}\frac{a_y}{a_x}\frac{h_x}{h_y}\right) \leq \frac{h_{\text{flow}}}{2|\boldsymbol{a}|}$$

$$\tau_{L_2}^e = \frac{\|b_0\|_{L_2(\Omega^e)}}{\text{meas}(\Omega)^{e\,1/2}} = \frac{h_{\text{flow}}}{\sqrt{3}|\boldsymbol{a}|}\sqrt{1 - \frac{1}{2}\frac{a_y}{a_x}\frac{h_x}{h_y}} \leq \frac{h_{\text{flow}}}{\sqrt{3}|\boldsymbol{a}|}$$

where h_{flow} is the longest length of the element along the streamwise direction.

Remarks.

1. The above upper bound for the L_1 error scale, calculated here for the rectangular bilinear quad and any velocity direction, was suggested by [91]. An attempt to include flow directionality into the flow intrinsic time scale was given in [93].
2. For $\theta = 0$, the one-dimensional error time scales are recovered.
3. Let us recall that in 1D $\tau_{\text{flow}} = \tau_{L_1}$ [78].

Elliptic limit. In the elliptic limit, the residual-free-bubble is the solution of the problem

$$\begin{cases} \kappa \Delta b_0^e = 1 & \text{in} \quad \Omega^e \\ b_0^e = 0 & \text{on} \quad \Gamma^e \end{cases}$$

where κ is the diffusion coefficient.

The solution, depicted in Fig. 4, can be expressed as the series [94]

$$b_0^e(\boldsymbol{x}) = \frac{16}{\pi^4 \kappa} \sum_{m=1(\text{odd})}^{\infty} \sum_{n=1(\text{odd})}^{\infty} \frac{1}{\frac{n^2}{h_x^2} + \frac{m^2}{h_y^2}} \frac{1}{nm} \sin\left(\frac{n\pi}{h_x} x\right) \sin\left(\frac{m\pi}{h_y} y\right) \tag{32}$$

which leads to the following error time scales:

$$\tau_{L_1} = \frac{64}{\pi^6 \kappa} \sum_{m=1(\text{odd})}^{\infty} \sum_{n=1(\text{odd})}^{\infty} \frac{1}{\frac{n^2}{h_x^2} + \frac{m^2}{h_y^2}} \frac{1}{(nm)^2} \tag{33}$$

$$\tau_{L_2} = \frac{8}{\pi^4 \kappa} \sqrt{\sum_{m=1(\text{odd})}^{\infty} \sum_{n=1(\text{odd})}^{\infty} \frac{1}{\left(\frac{n^2}{h_x^2} + \frac{m^2}{h_y^2}\right)^2} \frac{1}{(nm)^2}} \tag{34}$$

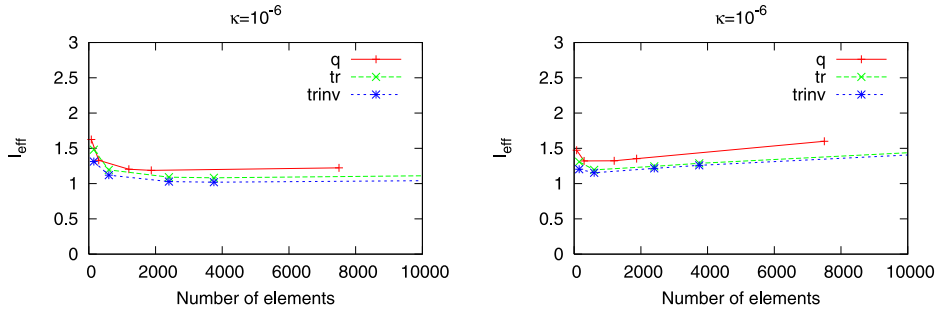

Fig. 5. L-shaped domain problem. Efficiencies for the L_1 (left) and L_2 (right) norms for various types of two-dimensional elements. Advection dominated flow. (q = quads, tr = triangles, trinv = triangles with the diagonal in opposite direction).

Remarks.

1. The error scales for $h_x = h_y$ are calculated as
$$\tau_{L_1} = \frac{h_x^2}{28.45\kappa} \qquad \tau_{L_2} = \frac{h_x^2}{24.24\kappa} \tag{35}$$
2. Note that the error time scales are approximately half of the one-dimensional diffusive flow time scale.
3. The error time scales for the L_1 and L_2 norms are similar.
4. For the reaction limit, see [75].
5. Chacon and coworkers [95–98] incorporate the above error time scales as stabilization parameters, showing very good properties of accuracy and stability.

2.7. Two-dimensional example

We show here some results based on the L-shaped domain problem, described in [58], with zero essential boundary conditions along the domain boundary. The parameters of the problem are $\boldsymbol{a} = (1, 3)$, two values of $\kappa = 10^{-6}, 1$, $s = -1$ and the independent force term $f(x)$,

$$f(x, y) = 100r(r - 0.5)(r - 1/\sqrt{2}) \tag{36}$$

with $r^2 = (x - 0.5)^2 + (y - 0.5)^2$.

Figs. 5–6 show that global and local efficiencies very closed to one are attained for both, advection and diffusion dominated flows, for various element types and shapes [75]. In Fig. 6, the zones where the efficiency is large correspond to places with very small exact and estimated errors (of the order of 10^{-7} [75]), where at the same time, the efficiency index losses its significance as it is the ratio of two very small quantities.

2.8. Application to adaptivity

As mentioned before, it is possible to create adaptive strategies in order to adjust the mesh size in the problem domain and, thus, optimize the computational time. Given an error tolerance, $e_{\text{tol}} = \|u - \bar{u}\|_{(\Omega^e)} = \|u'_{\text{tol}}\|_{(\Omega^e)}$, the local norm of the estimated error $\eta_{L_2}^{e(i)} \approx \|u'\|_{(\Omega^e)}$ at iteration (i), and the mesh size distribution $h^{e(i)}$ at iteration (i), it can be shown that the new mesh size distribution at iteration $(i + 1)$ is

$$h^{e(i+1)} = \left[\frac{e_{\text{tol}}}{\eta_{L_2}^{e(i)}}\right]^{1/p} h^{e(i)} \tag{37}$$

with p the order of convergence of the solution. In our case, although more efficient strategies are available using coarsening and refining algorithms, at each iteration the mesh is regenerated using a commercial mesh generator. For other norms and remeshing strategies, the interested reader is referred to [99].

The L-shaped problem is a common benchmark applied to the transport equation. Fig. 7 illustrates the initial mesh of the problem whereas the image on the right shows the final adapted mesh, which captures the boundary, outflow and interior layers for a high Peclet number case with $\kappa = 10^{-6}$ (see [99] for more details).

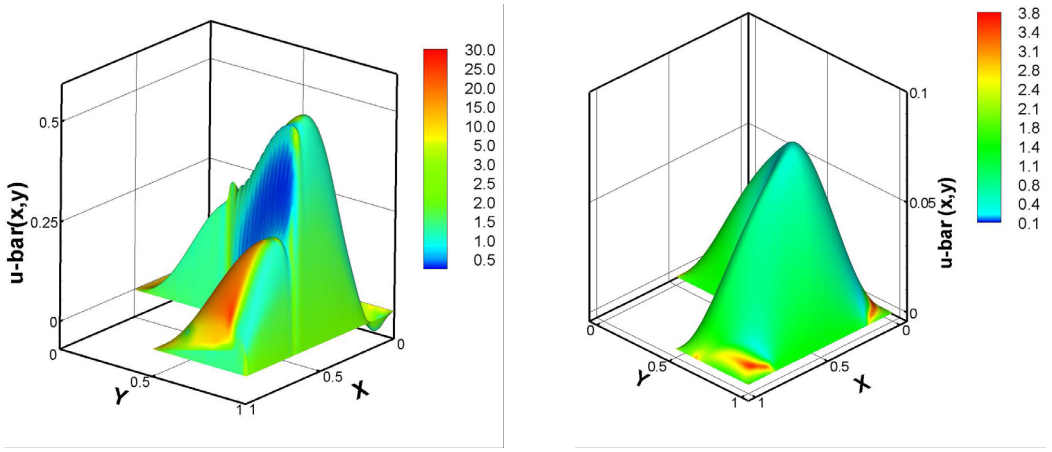

Mesh $h_x = 0.01$.

Fig. 6. L-shaped domain problem. Local efficiencies for the L_2 norm plotted over the finite element solution. Advection dominated flow (left), Diffusion dominated flow (right).

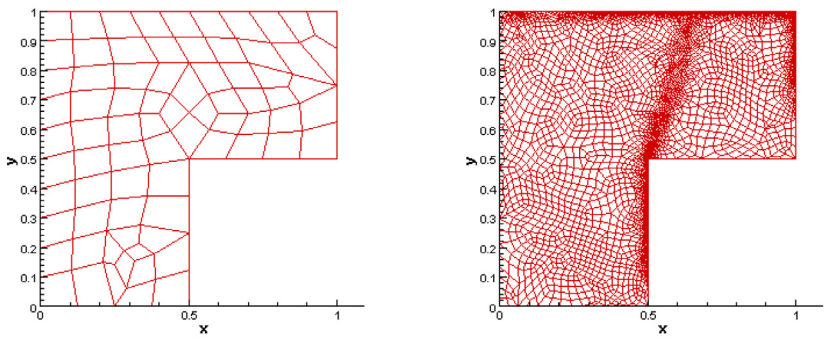

(a) Initial mesh (b) Final mesh

Fig. 7. Adapted mesh for the L-shaped problem generated using VMS.

2.9. Application to quantities of interest

In [100] the present theory was successfully applied to estimate the error for quantities of interest, obviating the need of computing the dual problem. [101] confirmed that the explicit error estimates obtained with the present method coincide with those calculated combining the primal and dual problems. However, in order to generate adapted meshes based on a quantity of interest, the adapted mesh should also be driven by the dual problem.

It is noteworthy that Garg and Stogner [68] use VMS fine-scale information to enhance the accuracy of the computed quantities of interest, providing superior rates of convergence, including exact recovery for a non-trivial class of quantities of interest.

2.10. Further works

Initial steps for using directly the subgrid scales to estimate the error can be found in [81,102–105], where the subscales are computed in larger patches with homogeneous Dirichlet boundary conditions.

VMS error estimation for the advection–diffusion was applied to fluid problems in [106–110]. An application to refinement algorithms for Isogeometric Analysis can be found in [66,67].

3. Hyperbolic problems: the Euler and Navier–Stokes equations

The previous ideas are extended to hyperbolic problems, simply by diagonalizing the system and applying the formulation to the diagonal equations. This is exact for one-dimensional systems with constant coefficient matrices, whereas it is an approximation for nonlinear or multidimensional cases. A more detailed explanation can be found in [111].

3.1. Preliminaries

Consider an open spatial domain Ω with boundary Γ, such that $\Gamma = \Gamma_{\mathcal{G}} \cup \Gamma_{\mathcal{H}}$. The *strong form* of the boundary-value problem consists of finding the solution vector $\boldsymbol{Y} : \Omega \to \mathbb{R}^{n_{\text{eq}}}$, where n_{eq} is the number of equations of the system (which coincides with the number of unknowns), such that for the given essential boundary conditions $\boldsymbol{\mathcal{G}} : \Gamma_{\mathcal{G}} \to \mathbb{R}^{n_{\text{eq}}}$ and the natural boundary conditions $\boldsymbol{\mathcal{H}} : \Gamma_{\mathcal{H}} \to \mathbb{R}^{n_{\text{eq}}}$, the following equations are satisfied

$$\left\{\begin{array}{rcll} \boldsymbol{\mathcal{L}}\boldsymbol{Y} & = \boldsymbol{0} & \text{in} & \Omega \\ \boldsymbol{Y} & = \boldsymbol{\mathcal{G}} & \text{on} & \Gamma_{\mathcal{G}} \\ \boldsymbol{\mathcal{B}}\boldsymbol{Y} & = \boldsymbol{\mathcal{H}} & \text{on} & \Gamma_{\mathcal{H}} \end{array}\right. \tag{38}$$

More complex boundary conditions could be contemplated with simple extensions of the theory. Here $\boldsymbol{\mathcal{L}}$ represents a steady linear second order vector operator, such as the advective–diffusive system

$$\boldsymbol{\mathcal{L}}\boldsymbol{Y} = \boldsymbol{A}_i \boldsymbol{Y}_{,i} + (\boldsymbol{K}_{ij}\boldsymbol{Y}_{,j})_{,j} - \boldsymbol{S} \tag{39}$$

where $\boldsymbol{A}_i$ are constant Euler Jacobians, $\boldsymbol{K}_{ij}$ constant diffusion matrices and $\boldsymbol{S}$ a linear source term. Many systems admit a conservative form, which can be expressed as [112,113]

$$\boldsymbol{\mathcal{L}}\boldsymbol{Y} = \boldsymbol{F}^{\text{adv}}_{i,i} - \boldsymbol{F}^{\text{diff}}_{i,i} - \boldsymbol{S} \tag{40}$$

where $\boldsymbol{F}^{\text{adv}}_i$ is the ith advective flux with $\boldsymbol{A}_i = \boldsymbol{F}^{\text{adv}}_{i,\boldsymbol{Y}}$ and $\boldsymbol{F}^{\text{diff}}_i$, the ith diffusive flux, with $\boldsymbol{F}^{\text{diff}}_i = \boldsymbol{K}_{ij}\boldsymbol{Y}_{,j}$.

Remark. For the Euler and Navier–Stokes equations, $\boldsymbol{\mathcal{L}}$ can be taken as the quasilinear form of the equations, which represents a linearization of the system.

Next, consider the *conservative weak* form: Find $\boldsymbol{Y} \in \boldsymbol{\mathcal{S}}$ such that $\forall \boldsymbol{W} \in \boldsymbol{\mathcal{V}}$

$$-(\boldsymbol{W}_{,i}, \boldsymbol{F}^{\text{adv}}{}_i) + (\boldsymbol{W}_{,i}, \boldsymbol{F}^{\text{diff}}{}_i) = (\boldsymbol{W}, \boldsymbol{S}) + (\boldsymbol{W}, \boldsymbol{\mathcal{H}})_{\Gamma_{\mathcal{H}}} \tag{41}$$

where $\boldsymbol{\mathcal{S}}$ and $\boldsymbol{\mathcal{V}}$ are the corresponding solution and weighting spaces,

$$\begin{array}{rcl} \boldsymbol{\mathcal{S}} & = & \{\boldsymbol{Y} \mid \boldsymbol{Y} \in (H^1)^{n_{\text{eq}}},\ \boldsymbol{Y} = \boldsymbol{\mathcal{G}} \text{ on } \Gamma_{\mathcal{G}}\} \\ \boldsymbol{\mathcal{V}} & = & \{\boldsymbol{W} \mid \boldsymbol{W} \in (H^1)^{n_{\text{eq}}},\ \boldsymbol{W} = \boldsymbol{0} \text{ on } \Gamma_{\mathcal{G}}\} \end{array} \tag{42}$$

and the natural boundary condition is given by the operator

$$\boldsymbol{\mathcal{B}}\boldsymbol{Y} = -\boldsymbol{F}^{\text{adv}}_i n_i + \boldsymbol{F}^{\text{diff}}_i n_i \tag{43}$$

with $\boldsymbol{n} = [n_i]$, the outward normal to the boundary.

3.2. The error estimation paradigm

Following the same steps as in Section 2.2, a sum decomposition is introduced for the *exact solution* $\boldsymbol{Y} \in \boldsymbol{\mathcal{S}} \subset H^1$ into the *finite element solution* (resolved or subgrid scales) $\overline{\boldsymbol{Y}}$ and the *error* (unresolved scales) $\boldsymbol{Y}'$, and likewise for the weighting function [4,5],

$$\begin{array}{rcl} \boldsymbol{Y} & = \overline{\boldsymbol{Y}} + \boldsymbol{Y}' \\ \boldsymbol{W} & = \overline{\boldsymbol{W}} + \boldsymbol{W}' \end{array} \tag{44}$$

Typically $\overline{\boldsymbol{Y}}$ belongs to a finite element space $\bar{\boldsymbol{\mathcal{S}}}$ with Ω^e, $e = 1, \ldots, n_{\text{el}}$ disjoint elements. The union of element interiors is denoted by $\widetilde{\Omega} = \cup_e^{n_{\text{el}}} \Omega^e$ whereas the inter-element boundaries, by $\widetilde{\Gamma} = \cup_e^{n_{\text{el}}} \Gamma^e \setminus \Gamma$ with Γ^e the element boundary. Accordingly, the error $\boldsymbol{Y}' \in \boldsymbol{\mathcal{S}}'$ with $\boldsymbol{\mathcal{S}}' = \boldsymbol{\mathcal{S}}/\bar{\boldsymbol{\mathcal{S}}}$ [70].

The above splitting is substituted into the weak form and invoking linearity, Eq. (41) is equivalent to two subproblems,

$$-(\overline{\boldsymbol{W}}_{,i}, \boldsymbol{F}_i^{\text{adv}}) + (\overline{\boldsymbol{W}}_{,i}, \boldsymbol{F}_i^{\text{diff}}) = (\overline{\boldsymbol{W}}, \boldsymbol{S}) + (\overline{\boldsymbol{W}}, \boldsymbol{\mathcal{H}})_{\Gamma_{\mathcal{H}}} \tag{45a}$$

$$-(\boldsymbol{W}'_{,i}, \boldsymbol{F}_i^{\text{adv}}) + (\boldsymbol{W}'_{,i}, \boldsymbol{F}_i^{\text{diff}}) = (\boldsymbol{W}', \boldsymbol{S}) + (\boldsymbol{W}', \boldsymbol{\mathcal{H}})_{\Gamma_{\mathcal{H}}} \tag{45b}$$

The first subproblem is the equation for the coarse scales and the second one, the subproblem for the subgrid scales or error.

We are interested in deriving an equation for the error $\boldsymbol{Y}'$. Because of linearity, one can write

$$\begin{aligned} \boldsymbol{F}_i^{\text{adv}} &= \bar{\boldsymbol{F}}_i^{\text{adv}} + \boldsymbol{F}_i^{\text{adv}\prime} \\ \boldsymbol{F}_i^{\text{diff}} &= \bar{\boldsymbol{F}}_i^{\text{diff}} + \boldsymbol{F}_i^{\text{diff}\prime} \\ \boldsymbol{S} &= \bar{\boldsymbol{S}} + \boldsymbol{S}' \end{aligned} \tag{46}$$

Therefore, the second subproblem can be written as

$$\begin{aligned} -(\boldsymbol{W}'_{,i}, \boldsymbol{F}_i^{\text{adv}\prime}) + (\boldsymbol{W}'_{,i}, \boldsymbol{F}_i^{\text{diff}\prime}) - (\boldsymbol{W}', \boldsymbol{S}') = \\ (\boldsymbol{W}'_{,i}, \bar{\boldsymbol{F}}_i^{\text{adv}}) - (\boldsymbol{W}'_{,i}, \bar{\boldsymbol{F}}_i^{\text{diff}}) + (\boldsymbol{W}', \bar{\boldsymbol{S}}) + (\boldsymbol{W}', \boldsymbol{\mathcal{H}})_{\Gamma_{\mathcal{H}}} \end{aligned} \tag{47}$$

Now, the first two terms on the right-hand-side can be integrated by parts, that is,

$$\begin{aligned} (\boldsymbol{W}'_{,i}, \bar{\boldsymbol{F}}_i^{\text{adv}}) &= \sum_e (\boldsymbol{W}'_{,i}, \bar{\boldsymbol{F}}_i^{\text{adv}})_{(\Omega^e)} \\ &= \sum_e \left\{ -(\boldsymbol{W}', \bar{\boldsymbol{F}}_{i,i}^{\text{adv}})_{(\Omega^e)} + (\boldsymbol{W}', \bar{\boldsymbol{F}}_i^{\text{adv}} n_i)_{\Gamma^e} \right\} \\ &= -(\boldsymbol{W}', \bar{\boldsymbol{F}}_{i,i}^{\text{adv}})_{\widetilde{\Omega}} + (\boldsymbol{W}', [\![\bar{\boldsymbol{F}}_i^{\text{adv}} n_i]\!])_{\widetilde{\Gamma}} + (\boldsymbol{W}', \bar{\boldsymbol{F}}_i^{\text{adv}} n_i)_{\Gamma_{\mathcal{H}}} \end{aligned} \tag{48}$$

$$\begin{aligned} (\boldsymbol{W}'_{,i}, \bar{\boldsymbol{F}}_i^{\text{diff}}) &= \sum_e (\boldsymbol{W}'_{,i}, \bar{\boldsymbol{F}}_i^{\text{diff}})_{(\Omega^e)} \\ &= \sum_e \left\{ -(\boldsymbol{W}', \bar{\boldsymbol{F}}_{i,i}^{\text{diff}})_{(\Omega^e)} + (\boldsymbol{W}', \bar{\boldsymbol{F}}_i^{\text{diff}} n_i)_{\Gamma^e} \right\} \\ &= -(\boldsymbol{W}', \bar{\boldsymbol{F}}_{i,i}^{\text{diff}})_{\widetilde{\Omega}} + (\boldsymbol{W}', [\![\bar{\boldsymbol{F}}_i^{\text{diff}} n_i]\!])_{\widetilde{\Gamma}} + (\boldsymbol{W}', \bar{\boldsymbol{F}}_i^{\text{diff}} n_i)_{\Gamma_{\mathcal{H}}} \end{aligned} \tag{49}$$

where $[\![\cdot]\!]$ is the jump operator [5,69].

Substituting in the fine-scale problem (47), one arrives at

$$\begin{aligned} -(\boldsymbol{W}'_{,i}, \boldsymbol{F}_i^{\text{adv}\prime}) + (\boldsymbol{W}'_{,i}, \boldsymbol{F}_i^{\text{diff}\prime}) - (\boldsymbol{W}', \boldsymbol{S}') \\ = -(\boldsymbol{W}', \boldsymbol{\mathcal{L}}\overline{\boldsymbol{Y}} - \bar{\boldsymbol{S}})_{\widetilde{\Omega}} + (\boldsymbol{W}', [\![\bar{\boldsymbol{F}}_i^{\text{adv}} n_i]\!] - [\![\bar{\boldsymbol{F}}_i^{\text{diff}} n_i]\!])_{\widetilde{\Gamma}} \\ + (\boldsymbol{W}', \bar{\boldsymbol{F}}_i^{\text{adv}} n_i - \bar{\boldsymbol{F}}_i^{\text{diff}} n_i + \boldsymbol{\mathcal{H}})_{\Gamma_{\mathcal{H}}} \\ = -(\boldsymbol{W}', \boldsymbol{\mathcal{L}}\overline{\boldsymbol{Y}} - \bar{\boldsymbol{S}})_{\widetilde{\Omega}} - (\boldsymbol{W}', [\![\boldsymbol{\mathcal{B}}\overline{\boldsymbol{Y}}]\!])_{\widetilde{\Gamma}} \\ - (\boldsymbol{W}', \boldsymbol{\mathcal{B}}\overline{\boldsymbol{Y}} - \boldsymbol{\mathcal{H}})_{\Gamma_{\mathcal{H}}} \end{aligned} \tag{50}$$

Remarks.

1. As a consequence, it can be seen that the error is driven by the same partial differential equation as the primal problem but with a modified right-hand-side. The right-hand-side contains the sources of error: element interior residuals, inter-element flux jumps and natural boundary condition errors.
2. Errors associated with the Dirichlet boundary condition have been ignored.
3. For continuous solution finite element spaces, $\boldsymbol{F}_i^{\text{adv}}$ is also continuous because it is a function of the solution variables and, therefore, the jump of $\boldsymbol{F}_i^{\text{adv}}$ across inter-element boundaries is zero. This jump might have an impact in discontinuous Galerkin methods. However, $\boldsymbol{F}_i^{\text{diff}}$ contains derivatives of the solution variables and it is discontinuous even for continuous finite element spaces.

Then, solving analytically for $\boldsymbol{Y}'$ as a function of the fine-scale Green's function [5,75], the error of the numerical computation can be calculated by the following paradigm

$$\boxed{\begin{aligned}\boldsymbol{Y}'(\boldsymbol{x}) = \; & -\int_{\widetilde{\Omega}} \boldsymbol{G}'(\boldsymbol{x},\boldsymbol{y})\,(\boldsymbol{\mathcal{L}}\overline{\boldsymbol{Y}} - \bar{\boldsymbol{S}})(\boldsymbol{y})\,\mathrm{d}\Omega_y - \int_{\widetilde{\Gamma}} \boldsymbol{G}'(\boldsymbol{x},\boldsymbol{y})\,([\![\boldsymbol{\mathcal{B}}\overline{\boldsymbol{Y}}]\!])(\boldsymbol{y})\,\mathrm{d}\Gamma_y \\ & -\int_{\Gamma_{\mathcal{H}}} \boldsymbol{G}'(\boldsymbol{x},\boldsymbol{y})\,(\boldsymbol{\mathcal{B}}\overline{\boldsymbol{Y}} - \boldsymbol{\mathcal{H}})(\boldsymbol{y})\,\mathrm{d}\Gamma_y\end{aligned}} \tag{51}$$

where $\boldsymbol{G}'(\boldsymbol{x},\boldsymbol{y}) \in \boldsymbol{\mathcal{S}}' \times \boldsymbol{\mathcal{S}}'$ is the Green's function of the *fine-scale* problem [4,5], a matrix operator in this case, $[\![\cdot]\!]$ is the jump operator [5,69] and $\boldsymbol{x},\boldsymbol{y} \in \Omega$.

The fine-scale Green's function is the distribution that characterizes the behavior of the numerical error, and emanates from the proper projection of the global Green's function. Therefore, it depends on the differential operator (the partial differential equation with the corresponding geometry and boundary conditions), on the finite element space and on the method (or projector).

Remarks.

1. The interpolation errors of the boundary conditions have been neglected.
2. For the non-conservative form of the equations, the weak form can be written: Find $\boldsymbol{Y} \in \boldsymbol{\mathcal{S}}$ such that $\forall \boldsymbol{W} \in \boldsymbol{\mathcal{V}}$

$$(\boldsymbol{W}, \boldsymbol{F}^{\mathrm{adv}}_{i,i}) + (\boldsymbol{W}_{,i}, \boldsymbol{F}^{\mathrm{diff}}_{i}) = (\boldsymbol{W}, \boldsymbol{S}) + (\boldsymbol{W}, \boldsymbol{\mathcal{H}})_{\Gamma_{\mathcal{H}}} \tag{52}$$

where $\boldsymbol{\mathcal{S}}$ and $\boldsymbol{\mathcal{V}}$ are the corresponding solution and weighting spaces and the natural boundary condition is given by the operator

$$\boldsymbol{\mathcal{B}}\boldsymbol{Y} = \boldsymbol{F}^{\mathrm{diff}}_{i} n_i \tag{53}$$

with $\boldsymbol{n} = [n_i]$, the outward normal to the boundary. Then, the same error paradigm as (51) can be derived, but with $\boldsymbol{\mathcal{B}}$ given as above.

The error representation (51) can be split into errors stemming from element interior residuals and element boundary residuals [75], namely

$$\boldsymbol{Y}'(\boldsymbol{x}) = \boldsymbol{Y}'_{\mathrm{int}}(\boldsymbol{x}) + \boldsymbol{Y}'_{\mathrm{bnd}}(\boldsymbol{x}) \tag{54}$$

Using the triangle inequality, we can write for each component

$$\|Y'_i(\boldsymbol{x})\| \leq \|Y'_{i\,\mathrm{int}}(\boldsymbol{x})\| + \|Y'_{i\,\mathrm{bnd}}(\boldsymbol{x})\| \tag{55}$$

3.3. Summary of models

In this section, the proposed error estimators are summarized for convenience of the reader, distinguishing methods for hyperbolic systems and advection–diffusion systems.

Hyperbolic systems. There are three models:

1. Standard $r = 1,\ 2$

$$\boxed{\|Y'_i(x)\|_{L_r(\Omega^e)} \;\approx\; \|\tau_{\mathrm{flow}\,ij}\;(\boldsymbol{\mathcal{L}}\bar{\boldsymbol{Y}} - \boldsymbol{S})_j\|_{L_r(\Omega^e)} \qquad \text{on } \Omega^e} \tag{56}$$

where for the L_2 norm, $\boldsymbol{\tau}_{\mathrm{flow}}$ is substituted by $\boldsymbol{\tau}_{L_2}$.

2. Naive $r = 1,\ 2$

$$\boxed{\begin{aligned}\|Y'_i(x)\|_{L_r(\Omega^e)} \;&\leq\; \mathrm{meas}(\Omega^e)^{1/r} \quad \tau^{sm}_{L_r\;ij} \\ &\times\; \|(\boldsymbol{\mathcal{L}}\bar{\boldsymbol{Y}} - \boldsymbol{S})_j\|_{L_\infty(\Omega^e)} \qquad \text{on } \Omega^e\end{aligned}} \tag{57}$$

where τ^{sm}_{ij} is the signed maximum, that is the maximum absolute value within an element multiplied by its sign. In practice, the maximum value is searched from the collection of integration points.

3. Upper bound $r = 1,\ 2$

$$\boxed{\begin{aligned} \|Y_i'(x)\|_{L_r(\Omega^e)} &\leq \text{meas}(\Omega^e)^{1/r} \quad |\overline{\tau}^e_{L_r\, ij}| \\ &\times \|(\mathcal{L}\bar{\boldsymbol{Y}} - \boldsymbol{S})_j\|_{L_\infty(\Omega^e)} \qquad \text{on } \Omega^e \end{aligned}} \tag{58}$$

where $\overline{\tau}^e_{ij}$ is the average value of the parameter within an element. In practice, it can be calculated from the values at the integration points. It can be substituted by the maximum value within the element, but then, the upper bound results in a much higher error estimate.

Remarks.

1. Typically the Standard error estimator gives a smaller error estimate than the Naive model, which in turn gives a smaller error estimate than the Upper bound error estimator.
2. In practice, the L_∞ norm is computed as the maximum value at Gaussian quadrature points or nodal quadrature points. Using the nodal quadrature points results in higher error estimates, but it is less robust because at the boundary zero boundary condition values can be encountered.
3. Sources of approximation in these models are: the multi-dimensionality, the nonlinearity of the system of equations and the model for $\boldsymbol{\tau}$ (in the case of nondiagonalizable systems).

Advection–diffusion systems. There are three models:

1. Standard $r = 1,\ 2$

$$\boxed{\begin{aligned} \|Y_i'(x)\|_{L_r(\Omega^e)} &\approx \|\tau_{\text{flow}\, ij}\ (\mathcal{L}\bar{\boldsymbol{Y}} - \boldsymbol{S})_j\|_{L_r(\Omega^e)} \\ &+ \quad \text{meas}(\Omega^e)^{1/r} \quad \tau^+_{L_r\, ij} \\ &\quad \tfrac{1}{2}\frac{\text{meas}(\Gamma^e)}{\text{meas}(\Omega^e)} \quad \|[\![\boldsymbol{\mathcal{B}}\bar{\boldsymbol{Y}}]\!]_j\|_{L_\infty(\Gamma^e)} \qquad \text{on } \Omega^e \end{aligned}} \tag{59}$$

where (as for the inviscid case) for the L_2 norm, $\boldsymbol{\tau}_{\text{flow}}$ is substituted by $\boldsymbol{\tau}_{L_2}$, and $\tau^+_{ij} = \max^{\Omega^e}(0, \tau^e_{ij})$ calculated within the element.

2. Naive $r = 1,\ 2$

$$\boxed{\begin{aligned} \|Y_i'(x)\|_{L_r(\Omega^e)} &\leq \text{meas}(\Omega^e)^{1/r} \quad \tau^+_{L_r\, ij} \\ &\times \Big(\|(\mathcal{L}\overline{\boldsymbol{Y}} - \boldsymbol{S})_j\|_{L_\infty(\Omega^e)} \\ &\quad + \tfrac{1}{2}\frac{\text{meas}(\Gamma^e)}{\text{meas}(\Omega^e)} \quad \|[\![\boldsymbol{\mathcal{B}}\bar{\boldsymbol{Y}}]\!]_j\|_{L_\infty(\Gamma^e)} \Big) \quad \text{on } \Omega^e \end{aligned}} \tag{60}$$

where $\tau^+_{ij} = \max^{\Omega^e}(0, \tau^e_{ij})$ calculated within the element.

3. Upper bound $r = 1,\ 2$

$$\boxed{\begin{aligned} \|Y_i'(x)\|_{L_r(\Omega^e)} &\leq \text{meas}(\Omega^e)^{1/r} \quad |\tau^{ma}_{L_r\, ij}| \\ &\times \Big(\|(\mathcal{L}\overline{\boldsymbol{Y}} - \boldsymbol{S})_j\|_{L_\infty(\Omega^e)} \\ &\quad + \tfrac{1}{2}\frac{\text{meas}(\Gamma^e)}{\text{meas}(\Omega^e)} \quad \|[\![\boldsymbol{\mathcal{B}}\bar{\boldsymbol{Y}}]\!]_j\|_{L_\infty(\Gamma^e)} \Big) \quad \text{on } \Omega^e \end{aligned}} \tag{61}$$

where $\tau^{ma}_{ij} = \max^{(\Omega^e)}(|\tau^e_{ij}|)$ is the maximum value of the absolute value parameter within an element. In practice, it can be calculated from the values at the integration points.

3.4. Further works

Using VMS for error estimation in compressible flow simulation was further investigated in [114]. Some examples of adaptivity in the incompressible limit of the unified compressible–incompressible formulation [112,113] applied to thermal problems with natural convection can be found in [115]. [116,117] apply error estimates to boundary layer and unstructured mesh generation in ballistic applications with evolving geometries.

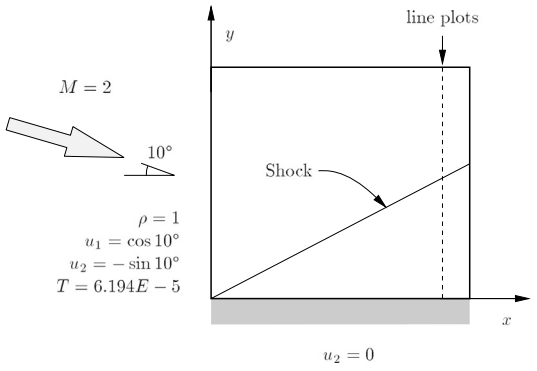

Fig. 8. Oblique shock problem setup.

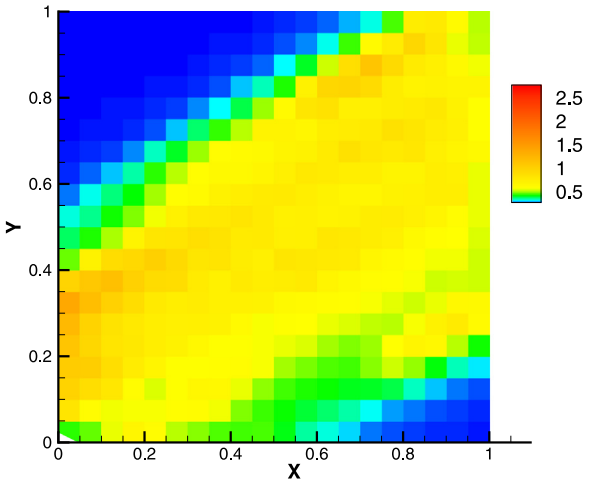

Fig. 9. Oblique shock problem. Naive error estimator. L_1 local efficiencies for T.

3.5. Numerical examples

To illustrate the performance of the a posteriori error estimator for the Euler and Navier–Stokes equations, the present formulation is applied to two inviscid examples (one supersonic and another one subsonic) and to a viscous low-Mach number case.

3.5.1. Oblique shock at M = 2

In this supersonic inviscid case, a uniform M = 2 flow is sharply turned 10° by a wall (see Fig. 8). Fig. 9 depicts the distribution of local efficiencies for temperature. It also shows that when changes in the solution are important, the local efficiency is about one. Table 1 summarizes the global efficiencies obtained by the three methods (see [111]).

3.5.2. Joukowski airfoil at M = 0.1

This example is devoted to the subsonic inviscid simulation of a Joukowski airfoil, with a dimensionless thickness t. Table 2 summarizes the efficiencies for p, u_1 and u_2 for the three estimators with an airfoil thickness $t = 0.15$. Fig. 10 shows an application of the error estimator to mesh adaptation based on the u_2 velocity component. For more information of the case description and for further results see [111].

Table 1
Oblique shock problem at $\mathrm{M} = 2$. Global efficiencies.

Model	norm	p	u_1	u_2	T
Standard	L_1	0.29	0.25	0.32	0.28
	L_2	0.31	0.28	0.34	0.31
Naive	L_1	0.74	0.76	0.88	0.92
	L_2	0.68	0.80	0.83	0.94
Upper bound	L_1	3.70	7.91	0.98	7.74
	L_2	3.30	7.42	0.91	7.29

Table 2
Joukowski airfoil at $\mathrm{M} = 0.1$, $t = 0.15$. Global efficiencies using a low Mach number tau based on [118].

Model	norm	p	u_1	u_2	T
Standard	L_1	0.63	0.17	0.67	–
	L_2	2.73	0.49	1.70	–
Naive	L_1	1.35	0.44	1.42	–
	L_2	4.92	1.00	3.38	–
Upper bound	L_1	1.63	0.99	1.30	–
	L_2	5.58	2.58	3.35	–

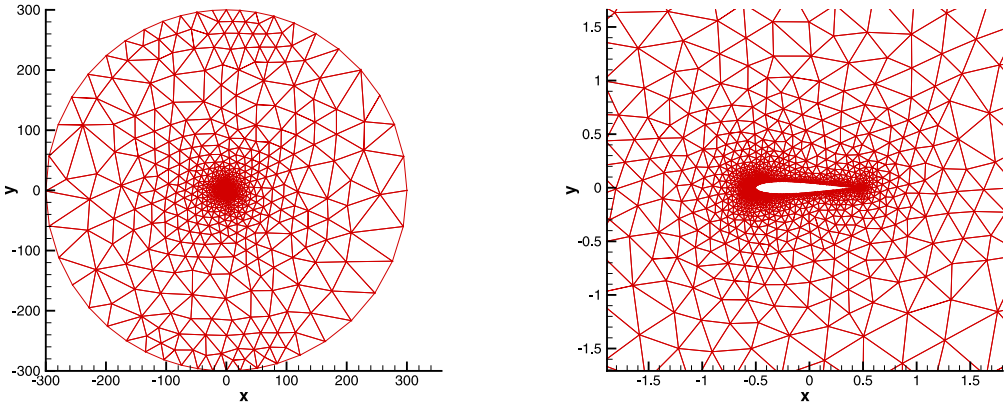

Fig. 10. Joukowski airfoil $\mathrm{M} = 0.1$, $t = 0.15$. Adapted mesh based on L_2 norm of u_2, $v_{\mathrm{tol}}/u_\infty = 0.001$.

3.5.3. Viscous boundary layer at $\mathrm{Re} = 10\,000$, $\mathrm{M} = 0.01$

In this final example, the formulation is applied to a viscous boundary layer (see Fig. 11 for the problem setup). Fig. 12 shows the local efficiencies of p, u_1 and u_2 obtained with the Naive method. Note that outside of the boundary layer, the exact and estimated errors are both very small and the effectivity index is not a reliable quantity.

4. Saddle-point problems: Stokes and Navier–Stokes equations

The concepts explained in the previous sections are extended to the Stokes and the incompressible Navier–Stokes equations. It is well known that saddle-point problems present some peculiarities that need to be taken into consideration. And although the Navier–Stokes are more demanding than the Stokes problem due to the presence of the convective term, both systems share many important traits.

In particular, the difficulties of calculating explicitly the fine-scale Green's function, made us take a different approach to calculate the error time-scales. Residuals and solution error are linked in a way inspired by VMS, that is, by multiplying the residuals with the corresponding error time-scales (or inverse-velocity scales in the case of H^1 seminorms), τ's. However, these τ's are computed a-priori from unitary problems.

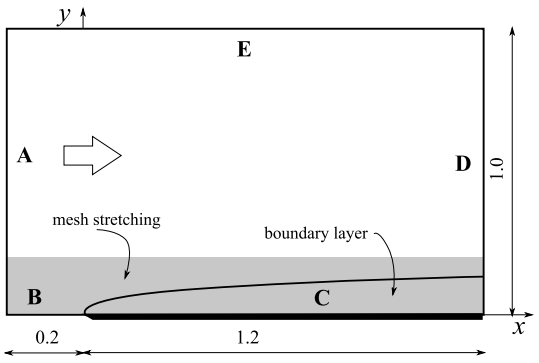

Fig. 11. Compressible boundary layer. Problem setup.

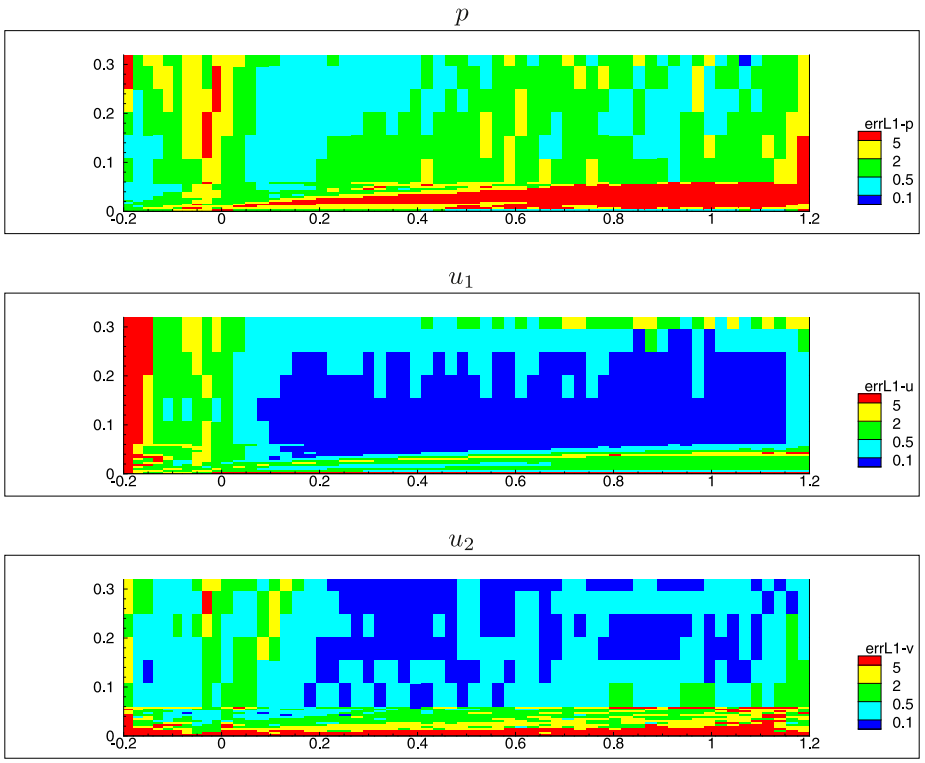

Fig. 12. Local efficiencies in a compressible boundary layer. L_1 norm, Naive method.

In this work, the problem is treated as a saddle point problem, thus, considering the pressure a Lagrange multiplier and focusing the efforts on the analysis of the error in the velocity field. The error estimation is analyzed in problems that reach the steady state; thus, turbulent flows at high Reynolds numbers are not handled. An extended explanation of this work is found in [119,120].

4.1. Preliminaries

Let Ω be a domain in $\mathbb{R}^{n_{\text{sd}}}$ with boundary Γ, where n_{sd} is the number of spatial dimensions of the problem. In this case $n_{\text{sd}} = 2$. According to the boundary conditions, the boundary is partitioned in two parts: Γ_g, where Dirichlet

boundary conditions are imposed and Γ_h, where Neumann boundary condition are defined, such that $\Gamma_g \cup \Gamma_h = \Gamma$ and $\Gamma_g \cap \Gamma_h = \emptyset$. The steady incompressible Navier–Stokes equations read

$$\left\{\begin{array}{rcll} \boldsymbol{u}\cdot\nabla\boldsymbol{u} + \nabla p - \nu\nabla^2\boldsymbol{u} & = \boldsymbol{f} & \text{in} & \Omega \\ \nabla\cdot\boldsymbol{u} & = \boldsymbol{0} & \text{in} & \Omega \\ \boldsymbol{u} & = \mathbf{g} & \text{on} & \Gamma_g \\ \mathcal{B}\boldsymbol{u} = \nu\nabla\boldsymbol{u}\cdot\boldsymbol{n} & = \boldsymbol{h} & \text{on} & \Gamma_h \end{array}\right. \tag{62}$$

where $\boldsymbol{u} = (u, v)$ and p are the unknown variables. $\boldsymbol{u}$ represents the velocity vector and ν the kinematic viscosity, which is assumed constant. In this work, we call p the pressure although, in fact, $p = \frac{p_{\text{mech}}}{\rho}$ where p_{mech} is the mechanical pressure and ρ is the density, that is considered constant. Finally, $\mathbf{g} = (g_x, g_y)^T$ and $\boldsymbol{h} = (h_x, h_y)^T$ are the Dirichlet and Neumann boundary conditions, respectively. When the viscosity is constant, the viscous term can be written as a Laplacian. In this simpler form, the above natural condition possesses a physical meaning, namely, the variation of the velocity in the outward normal direction of the boundary. In doing so, we avoid boundary conditions on pseudo-tractions, which lack physical meaning (see for instance [121,122]).

In short, problem (62) can be expressed as

$$\left\{\begin{array}{rcll} \mathcal{L}\boldsymbol{Y} & = \boldsymbol{S} & \text{in} & \Omega \\ \boldsymbol{u} & = \mathbf{g} & \text{on} & \Gamma_g \\ \mathcal{B}\boldsymbol{u} & = \boldsymbol{h} & \text{on} & \Gamma_h \end{array}\right. \tag{63}$$

where $\mathcal{L}$ is the equation differential operator, $\mathcal{B}$ is the differential operator which acts on the Neumann boundaries and arises from integration by parts. $\boldsymbol{Y} = (u, p, v)^T$ is the unknown vector and $\boldsymbol{S} = (f_x, 0, f_y)^T$ represents the source term.

The variational form is obtained multiplying the strong form by weighting functions and integrating by parts. To set it up we need to introduce the velocity weighting and trial solution spaces, $\mathcal{V}$ and $\mathcal{S}$, and the pressure weighting and trial spaces, $\mathcal{Q}$ and $\mathcal{P}$. Indeed,

$$\begin{array}{ll} \mathcal{V} & = \left\{\boldsymbol{v} \in (H^1(\Omega)^{n_{\text{sd}}}) \;\mid\; \boldsymbol{v} = \boldsymbol{0} \;\text{ on }\; \Gamma_g\right\} \\ \mathcal{S} & = \left\{\boldsymbol{u} \in (H^1(\Omega)^{n_{\text{sd}}}) \;\mid\; \boldsymbol{u} = \mathbf{g} \;\text{ on }\; \Gamma_g\right\} \\ \mathcal{Q} & = \left\{q \in L^2(\Omega) \cap H^1(\Omega) \quad \text{s.t.} \quad \int_\Omega q = 0\right\} \\ \mathcal{P} & = \left\{p \in L^2(\Omega) \cap H^1(\Omega) \quad \text{s.t.} \quad \int_\Omega p = 0\right\} \end{array} \tag{64}$$

The variational form can be written as: Find $\{\boldsymbol{u}, p\} \in \mathcal{S} \times \mathcal{P}$ such that

$$B(\boldsymbol{u}, p; \boldsymbol{v}, q) = F(\boldsymbol{v}, q), \forall\{\boldsymbol{v}, q\} \in \mathcal{V} \times \mathcal{Q} \tag{65}$$

with

$$B(\boldsymbol{u}, p; \boldsymbol{v}, q) = (\boldsymbol{u}\cdot\nabla\boldsymbol{u}, \boldsymbol{v}) + (\nabla p, \boldsymbol{v}) + \nu(\nabla\boldsymbol{u}, \nabla\boldsymbol{v}) - (\nabla\cdot\boldsymbol{u}, q) \tag{66}$$

and

$$F(\boldsymbol{v}, q) = (\boldsymbol{v}, \boldsymbol{f}) + (\boldsymbol{v}, \boldsymbol{h})_{\Gamma_h} \tag{67}$$

Note that in order to obtain the above natural boundary condition, the pressure term has not been integrated by parts.

Now, in order to establish the FEM formulation, we select finite dimensional spaces. Let $\mathcal{S}_h \subset \mathcal{S}$ and $\mathcal{V}_h \subset \mathcal{V}$ be the trial and weighting finite dimensional spaces for the velocity. Similarly, we define $\mathcal{P}_h \subset \mathcal{P}$ and $\mathcal{Q}_h \subset \mathcal{Q}$ as the trial and weighting finite dimensional spaces for the pressure. This spaces represent a partition $\mathscr{C}_h$ formed by elements Ω^e with boundary Γ^e.

The Galerkin method is set as: Find $\{\boldsymbol{u}_h, p_h\} \in \mathcal{S}_h \times \mathcal{P}_h$ such that

$$B(\boldsymbol{u}_h, p_h; \boldsymbol{v}_h, q_h) = F(\boldsymbol{v}_h, q_h), \;\; \forall\{\boldsymbol{v}_h, q_h\} \in \mathcal{V}_h \times \mathcal{P}_h \tag{68}$$

with

$$B(\boldsymbol{u}_h, p_h; \boldsymbol{v}_h, q_h) = (\boldsymbol{u}_h\cdot\nabla\boldsymbol{u}_h, \boldsymbol{v}_h) + (\nabla p_h, \boldsymbol{v}_h) + \nu(\nabla\boldsymbol{u}_h, \nabla\boldsymbol{v}_h) - (\nabla\cdot\boldsymbol{u}_h, q_h) \tag{69}$$

and

$$F(\boldsymbol{v}_h, q_h) = (\boldsymbol{v}_h, \boldsymbol{f}) + (\boldsymbol{v}_h, \boldsymbol{h})_{\Gamma_h} \tag{70}$$

Stabilized method. In order to obtain stable solutions, it is well known that the finite element spaces for velocity and pressure must satisfy the Babuška-Brezzi or inf-sup condition [123,124]. A way of circumventing this condition is to introduce stabilization terms in the discrete formulation. Besides, additional stabilized terms must be included in the FEM formulation since spurious oscillations can appear in the velocity field for convection-dominated regimes. Many authors have developed stabilized formulations for the Stokes problem [121,125–129] and Navier–Stokes [130–133].

In this work, the solution is driven towards steady state through a transient. Thus, following [134] the unsteady stabilized method reads: Find $\{\boldsymbol{u}_h, p_h\} \in \mathcal{S}_h \times \mathcal{P}_h$ such that

$$B_{\text{stab}}(\boldsymbol{u}_h, p_h; \boldsymbol{v}_h, q_h) = F_{\text{stab}}(\boldsymbol{v}_h, q_h), \ \forall \{\boldsymbol{v}_h, q_h\} \in \mathcal{V}_h \times \mathcal{P}_h \tag{71}$$

with

$$\begin{aligned} B_{\text{stab}}(\boldsymbol{u}_h, p_h; \boldsymbol{v}_h, q_h) = \ & (\frac{\partial \boldsymbol{u}_h}{\partial t}, \boldsymbol{v}_h) + (\boldsymbol{u}_h \cdot \nabla \boldsymbol{u}_h, \boldsymbol{v}_h) + (\nabla p_h, \boldsymbol{v}_h) + \\ & \nu(\nabla \boldsymbol{u}_h, \nabla \boldsymbol{v}_h) - (\nabla \cdot \boldsymbol{u}_h, q_h) + \\ & \sum_{\Omega^e \in \mathscr{C}_h} \tau_{\text{mom}} \left(\frac{\partial \boldsymbol{u}_h}{\partial t} + \boldsymbol{u}_h \cdot \nabla \boldsymbol{u}_h + \nabla p_h - \nu \Delta \boldsymbol{u}_h, \boldsymbol{u}_h \cdot \nabla \boldsymbol{v}_h \right. \\ & \left. + \nabla q_h - \nu \Delta \boldsymbol{v}_h \right)_{(\Omega^e)} + \delta (\nabla \cdot \boldsymbol{u}_h, \nabla \cdot \boldsymbol{v}_h) \end{aligned} \tag{72}$$

and

$$F_{\text{stab}}(\boldsymbol{v}_h, q_h) = (\boldsymbol{v}_h, \boldsymbol{f}) + (\boldsymbol{v}_h, \boldsymbol{h})_{\Gamma_h} + \sum_{\Omega^e \in \mathscr{C}_h} \tau_{\text{mom}} \big(\boldsymbol{f}, \boldsymbol{u}_h \cdot \nabla \boldsymbol{v}_h + \nabla q_h - \nu \Delta \boldsymbol{v}_h \big)_{(\Omega^e)} \tag{73}$$

where δ and τ_{mom} are stability parameters. They are taken from Codina [131]

$$\tau_{\text{mom}} = \left(\frac{c_1 \nu}{h^2} + \frac{c_2 |u|}{h} \right)^{-1} \qquad \delta = \frac{c_3 h^2}{\tau_{\text{mom}}} \tag{74}$$

The constants c_1, c_2 and c_3 are taken as $c_1 = 4$, $c_2 = 2$ and $c_3 = 1$. Note that other definitions exist that use the metric of the mesh, such as [113,135].

This stabilized formulation allows us to employ the same shape functions for the velocity and the pressure. Particularly, we select linear elements for triangles and bilinear elements for quadrilaterals.

4.2. The variational multiscale background

In the VMS framework, both the trial and test function spaces are decomposed into the resolved and unresolved subsets, $\mathcal{S} = \bar{\mathcal{S}} \oplus \mathcal{S}'$ and $\mathcal{V} = \bar{\mathcal{V}} \oplus \mathcal{V}'$. Due to the multiscale decomposition, the variables are divided into two parts such that

$$\begin{aligned} \boldsymbol{Y} &= \bar{\boldsymbol{Y}} + \boldsymbol{Y}' \qquad & \bar{\boldsymbol{Y}} \in \bar{\mathcal{S}}, \quad \boldsymbol{Y}' \in \mathcal{S}' \\ \boldsymbol{W} &= \bar{\boldsymbol{W}} + \boldsymbol{W}' \qquad & \bar{\boldsymbol{W}} \in \bar{\mathcal{V}}, \quad \boldsymbol{W}' \in \mathcal{V}' \end{aligned} \tag{75}$$

Thus, the variational formulation can be split into

$$B(\bar{\boldsymbol{u}}, \bar{p}; \bar{\boldsymbol{v}}, \bar{q}) + B(\boldsymbol{u}', p'; \bar{\boldsymbol{v}}, \bar{q}) = F(\bar{\boldsymbol{v}}, \bar{q}), \forall \{\bar{\boldsymbol{v}}, \bar{q}\} \in \bar{\mathcal{V}} \times \bar{\mathcal{Q}} \tag{76a}$$

$$B(\bar{\boldsymbol{u}}, \bar{p}; \boldsymbol{v}', q') + B(\boldsymbol{u}', p'; \boldsymbol{v}', q') = F(\boldsymbol{v}', q'), \forall \{\boldsymbol{v}', q'\} \in \mathcal{V}' \times \mathcal{Q}' \tag{76b}$$

Remark. Due to the decomposition, the convective term is split into the following terms, $\boldsymbol{u} \cdot \nabla \boldsymbol{u} = \bar{\boldsymbol{u}} \cdot \nabla \bar{\boldsymbol{u}} + \bar{\boldsymbol{u}} \cdot \nabla \boldsymbol{u}' + \boldsymbol{u}' \cdot \nabla \bar{\boldsymbol{u}} + \boldsymbol{u}' \cdot \nabla \boldsymbol{u}'$ The first term on the RHS corresponds to the coarse scales whereas the last three terms, to the error. The last and the second-to-last terms are neglected with respect to the first term on the RHS since we suppose that $\|\boldsymbol{u}'\| \ll \|\bar{\boldsymbol{u}}\|$.

Now, in order to estimate the error, we turn our attention to the fine-scale equation Eq. (76b). The fine-scale variational form can be expressed as: Find $\boldsymbol{u}' \in \mathcal{S}'$ and $p' \in \mathcal{P}'$ such that

$$\begin{aligned}(\bar{\boldsymbol{u}} \cdot \nabla \boldsymbol{u}', \boldsymbol{w}') + (\nabla p', \boldsymbol{w}') + \nu(\nabla \boldsymbol{u}', \nabla \boldsymbol{w}') = \quad & (\boldsymbol{f} - \bar{\boldsymbol{u}} \cdot \nabla \bar{\boldsymbol{u}} - \nabla \bar{p} + \nu \Delta \bar{\boldsymbol{u}}, \boldsymbol{w}')_{\widetilde{\Omega}} \\ & -([\![\mathcal{B}\bar{\boldsymbol{u}}]\!]_E, \boldsymbol{w}')_{\widetilde{\Gamma}} \\ & -(\mathcal{B}\bar{\boldsymbol{u}} - \boldsymbol{h}, \boldsymbol{w}')_{\Gamma_h} \quad \forall \boldsymbol{w}' \in \mathcal{V}'\end{aligned} \tag{77}$$

$$(\nabla \cdot \boldsymbol{u}', q') = (-\nabla \cdot \bar{\boldsymbol{u}}, q') \ \ \forall q' \in \mathcal{P}' \tag{78}$$

where $\widetilde{\Omega}$ is the union of the element interiors and $\widetilde{\Gamma}$ is the internal element boundaries, i.e., $\widetilde{\Gamma} = \cup \Gamma^e \backslash \Gamma = \cup E \backslash \Gamma$, with E being the edges of the partition $\mathscr{C}_h$. Also, $[\![\cdot]\!]_E$ denotes the jump operator that takes into account the derivative discontinuities of $\frac{\partial \bar{\boldsymbol{u}}}{\partial \boldsymbol{n}}$ across the element edges. For a velocity field $\boldsymbol{u} = (u, v)^T$, and an edge shared by elements Ω^+ and Ω^-, it is defined as

$$[\![\mathcal{B}\bar{\boldsymbol{u}}]\!]_E = \nu(\nabla \bar{u}|_{\partial\Omega^+ \cap E} \cdot \boldsymbol{n}^+ + \nabla \bar{u}|_{\partial\Omega^- \cap E} \cdot \boldsymbol{n}^-, \nabla \bar{v}|_{\partial\Omega^+ \cap E} \cdot \boldsymbol{n}^+ + \nabla \bar{v}_{|_{\partial\Omega^- \cap E}} \cdot \boldsymbol{n}^-)^T \tag{79}$$

where $\boldsymbol{n}^+$ and $\boldsymbol{n}^-$ are the unit outward normal of elements Ω^+ and Ω^-, respectively.

On the LHS of Eqs. (77) and (78), there appear terms which only involve the fine scales, particularly, the error projected to the fine-scale test functions. On the RHS, we have the residuals of the numerical solution projected to the same fine-scale test functions. Again there appear three kinds of residuals: element internal residuals, inter-element residuals and Neumann boundary condition residuals. The first residuals are related to the non satisfaction of the differential equation $\mathcal{L}\bar{\boldsymbol{Y}} - \boldsymbol{f}$ inside each element. It can be seen as the difference between the numerical and the exact solution once the differential operator is applied, $\mathcal{L}\bar{\boldsymbol{Y}} - \mathcal{L}\boldsymbol{Y}$. The second and third residuals are assembled together because they emerge from the lack of continuity of the numerical solution on the element boundaries.

In this error estimator, as the VMS theory shows, the residuals and the error estimate are directly linked. The way to proceed is to obtain *error time scales*, τ's, which represent an average of the fine scales on the element. Classically, the intrinsic time-scale τ's have been identified with stabilization parameters. However, these τ's also are linked to the subgrid scales or error of the numerical solution.

Taking the fine-scale Eqs. (77), the local error estimation is carried out setting this problem on each element Ω^e,

$$\begin{cases} (\bar{\boldsymbol{u}} \cdot \nabla \boldsymbol{u}', \boldsymbol{w}')_{(\Omega^e)} + (\nabla p', \boldsymbol{w}')_{(\Omega^e)} + \nu(\nabla \boldsymbol{u}', \nabla \boldsymbol{w}')_{(\Omega^e)} & = (\boldsymbol{f} - \bar{\boldsymbol{u}} \cdot \nabla \bar{\boldsymbol{u}} - \nabla \bar{p} + \nu \Delta \bar{\boldsymbol{u}}, \boldsymbol{w}')_{(\Omega^e)} \\ & \quad -([\![\mathcal{B}\bar{\boldsymbol{u}}]\!]_E, \boldsymbol{w}')_{\widetilde{\Gamma}^e} \\ & \quad -(\mathcal{B}\bar{\boldsymbol{u}} - \boldsymbol{h}, \boldsymbol{w}')_{\Gamma^e \cap \Gamma_h} \quad \forall \boldsymbol{w}' \in \mathcal{V}' \\ (\nabla \cdot \boldsymbol{u}', q')_{(\Omega^e)} = (-\nabla \cdot \bar{\boldsymbol{u}}, q')_{(\Omega^e)} \ \ \forall q' \in \mathcal{P}' & \end{cases} \tag{80}$$

From Eq. (80) we can identify five kinds of residuals for an element,

$$\begin{aligned} &\mathcal{R}_{Mx} = f_x - \boldsymbol{u} \cdot \nabla \bar{u} - \partial_x \bar{p} + \nu \Delta \bar{u} \ \text{ on } \ \Omega^e \\ &\mathcal{R}_{My} = f_y - \boldsymbol{u} \cdot \nabla \bar{v} - \partial_y \bar{p} + \nu \Delta \bar{v} \ \text{ on } \ \Omega^e \\ &\mathcal{R}_C = \nabla \cdot \bar{\boldsymbol{u}} \ \text{ on } \ \Omega^e \\ &\mathcal{R}_{S_\perp} = \nu [\![\nabla \bar{\boldsymbol{u}} \cdot \boldsymbol{n}]\!] \cdot \boldsymbol{n} \ \text{ on } \ \partial E \in \Omega^e \\ &\mathcal{R}_{S_\parallel} = \nu [\![\nabla \bar{\boldsymbol{u}} \cdot \boldsymbol{n}]\!] \cdot \boldsymbol{n}_\parallel \ \text{ on } \ \partial E \in \Omega^e \end{aligned} \tag{81}$$

The residuals $\mathcal{R}_{Mx}$, $\mathcal{R}_{My}$, $\mathcal{R}_C$ represent the internal residual for the momentum equation and continuity equation, respectively. On the other hand, the residuals $\mathcal{R}_{S_\perp}$ and $\mathcal{R}_{S_\parallel}$ denote the inter-element residual due to the jumps of the FEM solution on the element boundaries. Particularly, $\mathcal{R}_{S_\perp}$ is the orthogonal component of the jump and $\mathcal{R}_{S_\parallel}$ the parallel component with respect to the element edge.

Thus, extending previous works on VMS error estimation [18,75–78,81,99–102,106,108,109,111,114,136–143], the error estimator is built as the sum products of each residual times the corresponding parameter, which will be explained later. Thus, a dimensionally consistent expression to compute the explicit error estimator in the H^1

seminorm is defined as

$$
\begin{aligned}
|\boldsymbol{u}'|_{H^1(\Omega^e)} \coloneqq & \frac{1}{\sqrt{|(\Omega^e)|}}(\tau)_{H^1}^{\boldsymbol{u}_{\mathcal{R}_{Mx}}} \sum_{i=1}^{n_{\text{bub}}} |(\mathcal{R}_{Mx}, v_{\text{bub}_i})_{\Omega^e}| + \\
+ & \frac{1}{\sqrt{|(\Omega^e)|}}(\tau)_{H^1}^{\boldsymbol{u}_{\mathcal{R}_{My}}} \sum_{i=1}^{n_{\text{bub}}} |(\mathcal{R}_{My}, v_{\text{bub}_i})_{\Omega^e}| + \\
+ & \frac{1}{\sqrt{|(\Omega^e)|}}(\tau)_{H^1}^{\boldsymbol{u}_{\mathcal{R}_{C}}} \sum_{i=1}^{n_{\text{bub}}} |(\mathcal{R}_{C}, v_{\text{bub}_i})_{\Omega^e}| + \\
+ & \sqrt{|\Omega^e|}(\tau)_{H^1}^{\boldsymbol{u}_{\mathcal{R}_{S_\perp}}} \sum_{i=1}^{n_{\text{edge}}} \frac{1}{l_i} |(\mathcal{R}_{S_\perp}, v_{\text{bub}_i})_{\Gamma^e}| + \\
+ & \sqrt{|\Omega^e|}(\tau)_{H^1}^{\boldsymbol{u}_{\mathcal{R}_{S_\parallel}}} \sum_{i=1}^{n_{\text{edge}}} \frac{1}{l_i} |(\mathcal{R}_{S_\parallel}, v_{\text{bub}_i})_{\Gamma^e}|
\end{aligned}
\tag{82}
$$

where l_i is the length of the edge i in the element Ω^e and $(\tau)_{H^1}^{\boldsymbol{u}_{\mathcal{R}_i}}$ is the error time scale for each residual, i.e., for $i = Mx, My, C, S_\perp, S_\parallel$. In order to be consistent with the definition of the τ's, we have included geometric factors of the measure of the element, $|\Omega^e|$, in each residual [1,5,78]. In Eq. (82) we can see that the residuals are projected into functions called v_{bub_i}. The functions v_{bub_i} are n_{bub} local bubble functions defined in the element and n_{edge} on the element edges, which are related to the solution of the subgrid problem and error time scales, τ's, see [119]. These functions are defined as:

- *Triangular elements:* Let λ_{T1}, λ_{T2}, λ_{T3} be the barycentric or area coordinates. Then,

$$
\begin{cases}
v_{\text{bub}_i} & = \lambda_{Ti} \cdot \lambda_{Tj} \text{ for } 1 \leq i < j \leq 3 \\
v_{\text{bub}_4} & = \lambda_{T1}\lambda_{T2}\lambda_{T3}
\end{cases}
\tag{83}
$$

  Thus, we have four bubble functions per element.

- *Quadrilateral elements:* Let λ_{Q1}, λ_{Q2}, λ_{Q3}, λ_{Q4} be the barycentric or area coordinates. Then,

$$
\begin{cases}
v_{\text{bub}_i} & = \dfrac{\lambda_{Q1}\lambda_{Q2}\lambda_{Q3}\lambda_{Q4}}{\lambda_{Qi}} \text{ for } 1 \leq i \leq 4 \\
v_{\text{bub}_5} & = \lambda_{Q1}\lambda_{Q2}\lambda_{Q3}\lambda_{Q4}
\end{cases}
\tag{84}
$$

  Thus, we have five bubble functions per element.

The rest of the section is devoted to explain the calculation of the τ's. In order to compute the error time-scales for the momentum equations, we consider two different contributions: one related to the convective term and another one connected to the solution of a local Stokes problem. The diffusion-dominated contribution is taken from the work on Stokes flow [119], $(\tau_{St})_{H^1}^{\boldsymbol{u}_{\mathcal{R}_i}}$. The advection-dominated contribution is taken from the one-dimensional analysis of the advection-diffusion equation in [78] for the H_1 seminorm. There, it is shown that the error inverse-velocity scale for the transport equation is

$$
\frac{1}{|\boldsymbol{u}_h|} \min(\sqrt{\alpha}, \frac{\alpha}{\sqrt{3}})
\tag{85}
$$

where $\alpha = h_e|\boldsymbol{u}_h|/(2\nu)$ is the element Reynolds number. Considering that the Stokes contribution already takes into account the diffusive limit, the final expression for the error scale can be simplified to

$$
(\tau)_{H^1}^{\boldsymbol{u}_{\mathcal{R}_i}} = \min\left(\frac{1}{|\boldsymbol{u}_h|} \frac{\alpha}{\sqrt{3}}, (\tau_{St})_{H^1}^{\boldsymbol{u}_{\mathcal{R}_i}} \right)
\tag{86}
$$

Once the elemental error is obtained, the global error (i.e. the error in the whole domain) can be computed as

$$
|\boldsymbol{u}'|_{H^1(\Omega)} = \left(\sum_{\forall \Omega^e \in \Omega} |\boldsymbol{u}'|^2_{H^1(\Omega^e)} \right)^{1/2}
\tag{87}
$$

Remarks.

1. The Stokes error scales τ_{St}'s represent a measure of the error on a element of unit area (measured in H^1-seminorm) produced by a determined unit residual. As quadrilaterals and triangles are employed, we have to compute τ's for both types of elements using a unit-area triangular domain and a unit-area rectangular domain, respectively. They are computed solving the problem below (88) on an element of unit area. That is,
   Find $(\boldsymbol{u}', p') \in (Q_B, P_B)$, that satisfies
   $$\begin{cases} (\nabla p', \boldsymbol{w}') + \nu(\nabla \boldsymbol{u}', \nabla \boldsymbol{w}') = \\ \qquad (\boldsymbol{f} - \nabla \bar{p} + \quad \nu \nabla^2 \bar{\boldsymbol{u}}, \boldsymbol{w}')_{\Omega^e} + \frac{1}{2}(\nu [\![\nabla \bar{\boldsymbol{u}} \cdot \boldsymbol{n}]\!], \boldsymbol{w}')_{\Gamma^e} + \\ \qquad (\boldsymbol{h} - \nu \nabla \bar{\boldsymbol{u}} \quad \cdot \boldsymbol{n}, \boldsymbol{w}')_{\Gamma_h} \quad \forall \boldsymbol{w}' \in Q_B \\ \qquad (\nabla \cdot \boldsymbol{u}', q') = \quad (-\nabla \cdot \bar{\boldsymbol{u}}, q') \quad \forall q' \in P_B \end{cases} \tag{88}$$
   where Q_B and P_B are the velocity and pressure spaces, respectively. The τ_{St}'s are calculated integrating the solution of the subgrid problem. For more information, see [43,44,119], where the shape functions are a combination of bubble functions and edge bubble functions. The selected finite element spaces for velocities, Q_B, and pressure, P_B, to solve the local problem (88), satisfy the Babuška-Brezzi condition.
2. The factor $\frac{1}{2}$ in the jump in Eq. (88), expresses the splitting of the residuals on the element boundary between the two elements that share the boundary [7,22,43,44].
3. The values of the Stokes τ_{St}'s are listed in [119]. Eq. (82) shows that a specific error scale corresponds to each type of residual. It turns out that the classic τ associated to the internal bubble is not enough to predict the error correctly. In fact, as can be seen that the τ_{St}'s related to edge bubbles provide a significant error contribution (see [144], where it is shown that for low order elements, the edge residuals dominate the error estimate). Thus, a simpler error estimator could be considered taking into account only the residuals on the element boundaries, $\mathcal{R}_{S_\perp}$ and $\mathcal{R}_{S_\parallel}$.
4. The extension of the error estimation to 3D problems can be made using the expression (82) and considering the residuals on the faces instead of the residuals on the element boundaries. As a first approximation, the τ's in [119] can be employed.
5. Note that for estimates in the H^1 seminorm, the inviscid limit of the inverse-velocity error scale does not converge to the inviscid inverse-velocity error scale. This is so because the slope of the solution in the layers increases as the viscosity decreases. As a consequence, the error scales in the H^1 seminorm cannot be composed from the error scales for the inviscid limit and those for the diffusive limit, but it has to be derived considering both components simultaneously.
6. For incompressible and Stokes flow [119,120], direct computation of the error scales from the stabilization matrix underestimates the actual error. Also, we had to recur to numerical computation of the error constants because they could not be obtained from the fine-scale Green's function.

4.3. Further works

The variational multiscale theory was employed by Song and coworkers [50] to estimate the error and generate adapted meshes, where local Dirichlet problems are solved to both obtain the stabilized term and estimate the error employed in the mesh refinement process. Zheng et al. [145] developed a simple error estimator based on a local projection which is used for driving adaptive meshes. Araya et al. made use of VMS a posteriori error estimation for the Stokes and Brinkman equations in [146].

In the field of finite volume methods, Colomés et al. [147] develop an explicit VMS error estimator where the fine scales are modeled by the flow subgrid time-scales.

[139,148] applied the estimator to aerothermal problems. [138] uses the VMS error estimation with the orthogonal subscales for incompressible flows using the stabilization matrix as an error time scale, which as shown here underestimates the local error. This last work was extended to adaptivity for viscoelastic flows in [149].

Finally, following these ideas, VMS has been applied to linear elasticity in [141–143]. In [150] VMS error estimation is extended to small deformation elasticity applied to contact mechanics with friction and in [151] to incompressible finite elasticity with quite success.

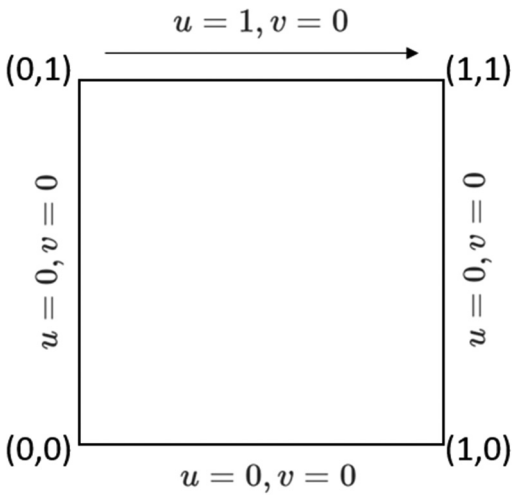

Fig. 13. Lid-driven cavity flow problem with unitary velocity on the top edge.

Table 3
Lid-driven cavity. Global efficiencies for velocity in H^1-seminorm for quadrilaterals and triangles.

n_{el}	Quadrilaterals			n_{el}	Triangles		
	Re = 1	Re = 100	Re = 1000		Re = 1	Re = 100	Re = 1000
16	2.717	2.482	2.433	32	0.845	0.825	0.795
64	3.404	2.798	2.048	128	1.192	1.136	1.125
256	3.305	2.693	1.887	512	1.263	1.150	0.932
1024	3.843	3.294	2.166	2048	1.294	1.210	0.921

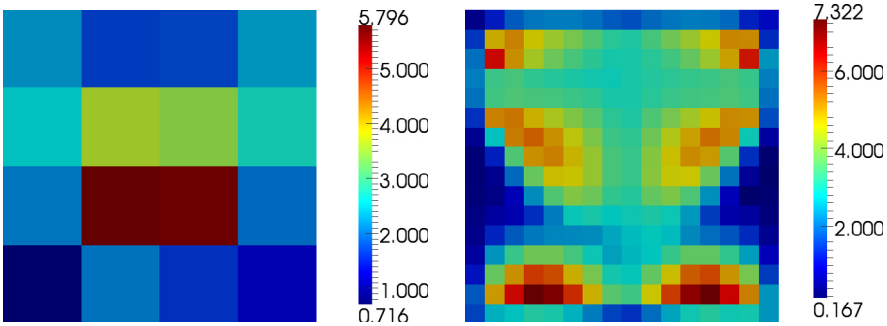

(a) $n_{el} = 16$ (b) $n_{el} = 256$

Fig. 14. Lid-driven cavity. Local efficiencies with the explicit error estimator. Re = 1.

4.4. Numerical example: Lid-driven cavity

The lid-driven cavity problem is a typical benchmark for viscous fluid flows. The domain is a unitary square consisting of three edges with no-slip conditions and a top edge with a unit tangential velocity (see Fig. 13). The pressure is set to zero at the lower left corner. As usual, the Reynolds number is based on the lid velocity and the square side length. Uniform meshes are considered.

Table 3 shows the global efficiencies for the considered estimators whereas Fig. 14 represents the local efficiencies for $n_{el} = 16$ and $n_{el} = 256$.

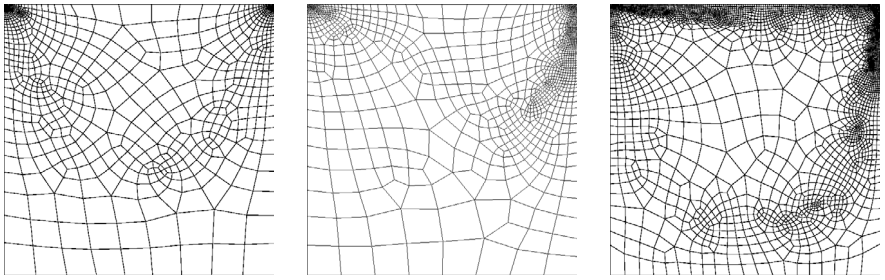

(a) Re=1 (b) Re=100 (c) Re=1000

Fig. 15. Lid-driven cavity. Adaptive mesh refinement for quadrilaterals. Re = 1, Re = 100 and Re = 1000.

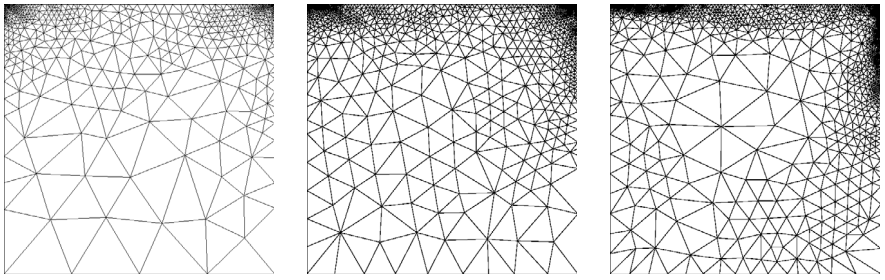

(a) Re=1 (b) Re=100 (c) Re=1000

Fig. 16. Lid-driven cavity. Adaptive mesh refinement for triangles. Re = 1, Re = 100 and Re = 1000.

Once the local error is estimated, we can evaluate where it is convenient to refine the mesh to obtain a more accurate solution. This remeshing process is made following Section 2.8, with an objective error tolerance of $\|u'_{TOL}\|_{H^1(\Omega^e)} = 0.080$. In Figs. 15 and 16, we observe how the elements are concentrated at the upper corners. The greater the Reynolds number, the finer the elements on the right side.

5. The nature of discrete error and pointwise error computation

This section is devoted to shedding light into the nature of the FEM error showing the connection between the residuals and the error itself. According to the nature of the residuals, the numerical error can be split into two components: element interior residuals and inter-element jumps. A relationship between these residuals (coarse scales) and the error components (fine scales) is established, yielding to a very simple model for the pointwise error, which is modeled as a linear combination of bubble functions for the element interior residuals and free-space Green's functions for the inter-element jumps. The numerical error is studied for the standard Galerkin and SUPG methods with application to the convection–diffusion equation.

5.1. Preliminaries

This section is based on the model, equations and definitions of Section 2. Again, the variational formulation reads: Find $u \in \mathcal{S}$ such that

$$a(w,u) = (w,f) + (w,h)_{\Gamma_h} \qquad \forall w \in \mathcal{V} \tag{89}$$

with the usual meaning for the bilinear forms operators, spaces and domains. Taking the elements of the partition, we define the associated finite dimensional spaces $\mathcal{S}^h \subset \mathcal{S}$ and $\mathcal{V}^h \subset \mathcal{V}$ for the trial and weighting functions, respectively,

$$\begin{aligned} \mathcal{S}^h &= \{u_h \in H^1(\Omega) \;\mid\; u_{h|\Omega^e} \in \mathbb{P}_k, u_{h|\Gamma_g} = g, \forall \Omega^e \in \widetilde{\Omega}\} \\ \mathcal{V}^h &= \{w_h \in H^1(\Omega) \;\mid\; w_{h|\Omega^e} \in \mathbb{P}_k, w_{h|\Gamma_g} = 0, \forall \Omega^e \in \widetilde{\Omega}\} \end{aligned} \tag{90}$$

where $\mathbb{P}_k$ denotes the space of polynomials of degree k. Thus, the standard Galerkin method reads: Find $u_h \in \mathcal{S}^h$ such that

$$a(w_h, u_h) = (w_h, f) + (w_h, h)_{\Gamma_h} \qquad \forall w_h \in \mathcal{V}^h \tag{91}$$

In order to stabilize the convection–diffusion equation, a popular method is SUPG, which includes an additional term to the Galerkin method. The SUPG method reads: Find $u_h \in \mathcal{S}^h$ such that

$$a_{\text{SUPG}}(w_h, u_h) = a(w_h, u_h) + a_\tau(w_h; u_h, f) = (w_h, f) + (w_h, h)_{\Gamma_h} \quad \forall w_h \in \mathcal{V}^h \tag{92}$$

The stabilizing term $a_\tau(\cdot;\cdot,\cdot)$ is

$$a_\tau(w_h; u_h, f) = \sum_{\Omega^e \in \widetilde{\Omega}} a^e_\tau(w_h; u_h, f) \tag{93}$$

where $a^e_\tau(w_h; u_h, f) = \big(\boldsymbol{a}\cdot\nabla w_h, \tau^e(\mathcal{L}u_h - f)\big)_{\Omega^e}$ and $\tau^e = \min\big(\frac{h}{2|\boldsymbol{a}|}, \frac{h^2}{12\kappa}\big)$. The value h is a measure of the element length.

The variational multiscale theory consists of splitting the variational form in a coarse and fine components. We identify the coarse scales with the finite element solution and the error with the fine scales. Therefore,

$$a(\bar{w}, \bar{u}) + a(\bar{w}, u') = (\bar{w}, f) + (\bar{w}, h)_{\Gamma_h} \qquad \forall \bar{w} \in \bar{\mathcal{V}} \tag{94a}$$

$$a(w', \bar{u}) + a(w', u') = (w', f) + (w', h)_{\Gamma_h} \qquad \forall w' \in \mathcal{V}' \tag{94b}$$

The spaces $\bar{\mathcal{V}}$ and $\bar{\mathcal{S}}$ represent the coarse scales and are identified with $\mathcal{V}^h$ and $\mathcal{S}^h$. The fine scales are defined such that $\mathcal{S} = \bar{\mathcal{S}} \oplus \mathcal{S}'$ and $\mathcal{V} = \bar{\mathcal{V}} \oplus \mathcal{V}'$.

Observing the variational multiscale form, Eq. ((94)a) represents the coarse-scale variational form and Eq. ((94)b), the fine-scale variational form. We focus on this last equation to estimate the error. Integrating by parts Eq. ((94)b), we establish the relationship between the error and the residuals,

$$a(w', u') = -(w', \mathcal{L}\bar{u} - f)_{\widetilde{\Omega}} - (w', [\![\mathcal{B}\bar{u}]\!])_{\widetilde{\Gamma}} - (w', \mathcal{B}\bar{u} - h)_{\Gamma_h} \tag{95}$$

The LHS of Eq. (95) is the bilinear form applied to the fine scales, where the error u' is projected on the fine scales w'. The RHS of Eq. (95) contains the residuals of the numerical solution. The first term of the RHS is the internal residuals defined inside the elements, the second one considers the jump of the flux on the element boundaries, and finally, the third term represents the Neumann boundary condition residual.

5.2. VMS error estimation framework

Following the nature of the residuals, the error is decomposed in two terms, u'_{bub} and u'_{poll}. Accordingly, the u'_{bub} component is in charge of modeling the error that arises from the internal residuals inside each element, $(w', \mathcal{L}\bar{u} - f)_{\Omega^e}$, and the u'_{poll} component represents the error produced by the residuals on the element boundary, $(w', [\![\mathcal{B}\bar{u}]\!])_{\widetilde{\Gamma}}$ and $(w', \mathcal{B}\bar{u} - h)_{\Gamma_h}$.

5.2.1. Internal residual error, u'_{bub}

This kind of error possesses a local character since it is defined inside the element. This error is computed as a combination of bubble functions on each element,

$$u'_{\text{bub},(\Omega^e)}(\boldsymbol{x}) = \sum_{i=1}^{n_{\text{bub}}} c_i^{\text{bub}} b_i(\boldsymbol{x}) \tag{96}$$

There are different ways of defining the bubble functions, $b_i(\boldsymbol{x})$, depending on whether we consider 1D and 2D problems.

One-dimensional problems. For 1D problems, the internal residual error is modeled by means of residual-free bubbles [4,5,82,84]. In this case, the residual-free bubbles are calculated using the fine-scale Green's functions. A relevant article written by Hughes and Sangalli [70] establishes an explicit definition of the fine-scale Green's operator,

$$\mathcal{G}' = \mathcal{G} - \mathcal{G}\mathcal{P}^T(\mathcal{P}\mathcal{G}\mathcal{P}^T)^{-1}\mathcal{P}\mathcal{G} \tag{97}$$

Eq. (97) shows that the fine-scale Green's operator is computed taking into account two terms, $\mathcal{G}$ and $\mathcal{P}$ (see [70,137] for further details):

- The classical Green's function operator, $\mathcal{G}$, which is the inverse of the differential equation, $\mathcal{G} = \mathcal{L}^{-1}$
- A projection, $\mathcal{P}$, that goes from the space of all scales, $\mathcal{S}$, to the coarse scales, $\bar{\mathcal{S}}$, $\mathcal{P} : \mathcal{S} \to \bar{\mathcal{S}}$. We select a projector induced by the H_0^1-seminorm since it provides fine-scale Green's functions confined in the elements.

Therefore, employing the fine-scale Green's functions, $g'(x, y)$, the internal residual error is computed as

$$u'_{\text{bub},\Omega^e}(x) = -\int_{\Omega^e} g'(x, y)(\mathcal{L}\bar{u} - f)(y)\, \mathrm{d}\Omega_y \tag{98}$$

In order to compute the error with bubble functions, we consider two cases

- Constant residual:

$$u'_{\text{bub},\Omega^e}(x) = b_0^e(x)(f - \mathcal{L}\boldsymbol{u}) \tag{99}$$

- Non-constant residual:

$$u'_{\text{bub},\Omega^e}(x) = b_0^e(x)(f - \mathcal{L}\bar{u})(c_i) + \sum_{k=1}^{\infty} b_k^e(x)\frac{1}{k!}\frac{d^k(f - \mathcal{L}\bar{u})}{dy^k}\bigg|_{y=c_i} \tag{100}$$

where c_i is the central point of the element and b_k^e is the k^{th}-moment order residual-free bubble, defined as

$$b_k^e(x) = \int_{\Omega^e} g'(x, y)(y - c_i)^k\, \mathrm{d}\Omega_y \tag{101}$$

These bubble functions, which arise from the fine-scale Green's function, are called *residual-free bubbles* since u'_{bub} fulfills

$$\int_{\Omega^e} \mathcal{L}u'_{\text{bub}} w'\, \mathrm{d}\Omega = \int_{\Omega^e} (f - \mathcal{L}\bar{u})w'\, \mathrm{d}\Omega \qquad \forall w' \in \mathcal{V}' \cap H_0^1(\Omega^e) \tag{102}$$

That is to say, in each element, u'_{bub} represents the solution that lives in $\mathcal{S}'$ with homogeneous Dirichlet boundary condition, where the source term is $f - \mathcal{L}\bar{u}$.

Multi-dimensional problems. In multidimensional problems, residual-free bubbles are very difficult to obtain. Thus, the error component, $u'_{\text{bub}}(\boldsymbol{x}) = \sum_{i=1}^{n_{bub}} c_i b_i(\boldsymbol{x})$ is a linear combination of polynomial bubble functions defined on a finite dimensional space, $\mathcal{S}^h_{\text{bub}}$. For both triangles and quadrilaterals, the first bubble function, $b_1(\boldsymbol{x})$, is the simplest polynomial that fulfills to be zero on the element boundary. The successive bubbles are built adding the monomials of the Pascal triangle with center in the barycenter of the element. The problem is set on each element as: Find $u'_{\text{bub}} \in \mathcal{S}^h_{\text{bub}}$ such that

$$a(w'_{\text{bub}}, u'_{\text{bub}}) = (w'_{\text{bub}}, f - \mathcal{L}\bar{u}) \qquad \forall w'_{\text{bub}} \in \mathcal{S}^h_{\text{bub}} \tag{103}$$

5.2.2. Inter-element error, u'_{poll}

The inter-element error presents a global character and is originated by the lack of continuity of the FEM solution, $\bar{u}$, and the internal residual error, u'_{bub}. This kind of error is in charge of solving the part of the error that u'_{bub} does not consider. Thus, the inter-element error, u'_{poll} represents the solution of the following problem,

$$\begin{cases} \mathcal{L}u'_{\text{poll}} &= 0 & \text{in} \quad \Omega \setminus \widetilde{\Gamma} \\ \mathcal{L}u'_{\text{poll}} &= -([\![\mathcal{B}\bar{u}]\!] + [\![\mathcal{B}u'_{\text{bub}}]\!])\delta_{\widetilde{\Gamma}} & \text{on} \quad \widetilde{\Gamma} \\ u'_{\text{poll}} &= 0 & \text{on} \quad \Gamma_g \\ \mathcal{B}u'_{\text{poll}} &= h - \mathcal{B}\bar{u} - \mathcal{B}u'_{\text{bub}} & \text{on} \quad \Gamma_h \end{cases} \tag{104}$$

It is assumed that the error component u'_{bub}, defined inside the elements, satisfies $\mathcal{L}u'_{\text{bub}} = f - \mathcal{L}\bar{u}$ enabling to approach $\mathcal{L}u'_{\text{poll}} = 0$ as the first equation in Eq. (104) expresses. Then, the error source is the jump of $\bar{u}$ and u'_{bub} on the element boundaries.

Although it seems that the way of determining the error pollution leads to the solution of a problem in the whole domain, it can be simplified both in 1D and multiD problems.

One-dimensional problems. Here only linear elements are considered (see [137] for the extension to higher-order elements). The error pollution is modeled as a linear combination of free-space Green's functions set at the nodes of the discretization, n_{np},

$$u'_{\text{poll}}(x) = \sum_{A=1}^{n_{np}} c_A^{\text{bnd}} g^F(x, x_A) \tag{105}$$

The coefficients c_A^{bnd} are determined depending on the nodes we are treating:

- Internal nodes
  The coefficients c_A^{bnd} are chosen imposing the Galerkin orthogonality property

  $$a(\boldsymbol{w}, u') = a(\boldsymbol{w}, u'_{\text{bub}}) + a(\boldsymbol{w}, u'_{\text{poll}}) = 0 \qquad \forall \boldsymbol{w} \in \bar{\mathcal{V}} \tag{106}$$

  Therefore,

  $$a(\boldsymbol{w}, u'_{\text{poll}}) = -a(\boldsymbol{w}, u'_{\text{bub}}) \qquad \forall \boldsymbol{w} \in \bar{\mathcal{V}} \tag{107}$$

  Introducing the definition of u'_{poll} in Eq. (105) and integrating by parts the LHS of Eq. (107), for a internal node A

  $$(\boldsymbol{w}_A, c_A^{\text{bnd}} \mathcal{L} g^F(x, x_A)) = -a(\boldsymbol{w}_A, u'_{\text{bub}}) \tag{108}$$

  $$(\boldsymbol{w}_A, \delta(x, x_A) c_A^{\text{bnd}}) = -a(\boldsymbol{w}_A, u'_{\text{bub}}) \tag{109}$$

  $$c_A^{\text{bnd}} = -a(\boldsymbol{w}_A, u'_{\text{bub}}) \tag{110}$$

- Neumann boundary nodes
  Following the same steps as for the internal nodes, the coefficients c_A^{bnd} at these nodes are computed as

  $$c_A^{\text{bnd}} = -a(\boldsymbol{w}_A, u'_{\text{bub}}) - \left(\boldsymbol{w}_A, \sum_{B=1, B\neq A}^{n_{np}} c_B^{\text{bnd}} \mathcal{B} g^F(x, x_B) \right)_{\Gamma_h} \tag{111}$$

- Dirichlet boundary nodes
  For the nodes set at the Dirichlet boundaries, we know that the $u' = 0$. Therefore, the c_A^{bnd} coefficients are solved imposing this condition, i.e.,

  $$c_A^{\text{bnd}} g^F(x_A, x_A) + \sum_{B=1, B\neq A}^{n_{np}} c_B^{\text{bnd}} g^F(x_A, x_B) = 0 \tag{112}$$

Multi-dimensional problems. Taking problem (104), the second equation is multiplied by the free-space Green's function and integrated by parts twice. Then, we get the expression

$$\begin{aligned} u'_{\text{poll}}(\boldsymbol{x}) = \; & -\int_{\widetilde{\Gamma}} g^F(\boldsymbol{x}, \boldsymbol{y}) \Big([\![\mathcal{B} \bar{u}]\!](\boldsymbol{y}) + [\![\mathcal{B} u'_{\text{bub}}]\!](\boldsymbol{y}) \Big) \, \mathrm{d}\Gamma_y + \\ & \int_{\partial\Omega} g^F(\boldsymbol{x}, \boldsymbol{y}) \mathcal{B}_y u'_{\text{poll}}(\boldsymbol{y}) \, \mathrm{d}\Gamma_y - \int_{\partial\Omega} u'_{\text{poll}}(\boldsymbol{y}) \mathcal{B}_y g^F(\boldsymbol{x}, \boldsymbol{y}) \, \mathrm{d}\Gamma_y \\ & \text{for all } \boldsymbol{x} \in \Omega \end{aligned} \tag{113}$$

As can be observed, the calculation of u'_{poll} implies the computation of an integral on the inter-element boundaries, $\widetilde{\Gamma}$, which involves the jumps of $\bar{u}$ and u'_{bub}. The other two integrals are set on the domain boundary and contain both u'_{poll} and its derivative. Hence, the integro-differential equation can be solved via boundary element methods (BEM).

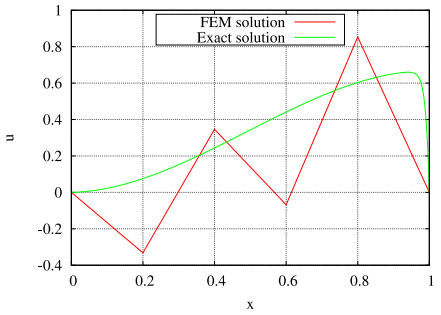

Fig. 17. 1D Convection–diffusion problem. Exact and FEM solution.

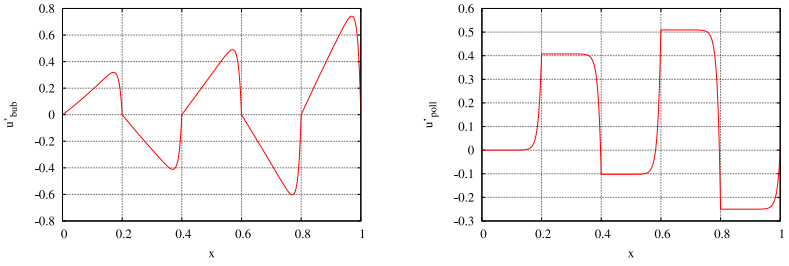

(a) u'_{bub} (b) u'_{poll}

Fig. 18. 1D Convection–diffusion problem. Error components.

5.3. Numerical examples

5.3.1. Pointwise error estimation in 1D problems

The convection–diffusion problem is expressed as

$$\begin{cases} -\kappa \dfrac{\mathrm{d}^2 u}{\mathrm{d}x^2} + a \dfrac{\mathrm{d}u}{\mathrm{d}x} = 4x(1-x) & \text{in} \quad \Omega = [0,1] \\ u = 0 & \text{on} \quad \Gamma_g \end{cases} \tag{114}$$

The case $\kappa = 0.01$ and $a = 1$ is solved with the standard Galerkin method using a uniform mesh with 5 elements. Fig. 17 represents the exact and the FEM solution, where spurious oscillations can be seen due to the regime being convection-dominated.

The error components u'_{bub} and u'_{poll} are depicted in Fig. 18. The interior error is estimated with Eq. (100) and the inter-element error is computed according to Section 5.2.2.

Finally, the estimated error is obtained summing both components, $u = u'_{\text{bub}} + u'_{\text{poll}}$. The estimated and the exact error are shown in Fig. 19. Both are almost identical.

5.3.2. Pointwise error estimation in 2D problems

The convection–diffusion problem in 2D is expressed as

$$\begin{cases} -\kappa \Delta u + \boldsymbol{a} \cdot \nabla u = f & \text{in} \quad \Omega \\ u = g & \text{on} \quad \Gamma_g \\ \kappa \nabla u \cdot \boldsymbol{n} = h & \text{on} \quad \Gamma_h \end{cases} \tag{115}$$

where κ and $\boldsymbol{a} = (a_x, a_y)$ are the diffusive and convection coefficients, respectively.

For the example, we select a $(0,1)\times(0,1)$-domain with $\kappa = 0.03$ and $\boldsymbol{a} = (1,2)/\sqrt{5}$ and homogeneous Dirichlet boundary conditions. We take $f = 1$. The numerical solution is obtained via the SUPG method employing a 8×8 mesh with bilinear quadrilaterals. The numerical and the reference solutions are shown in Fig. 20. The reference

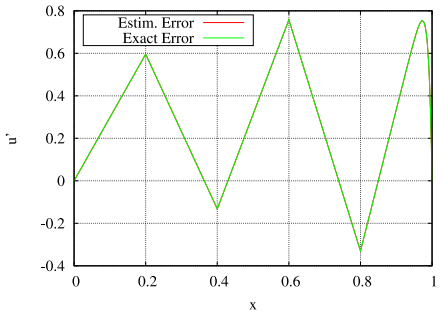

Fig. 19. 1D Convection–diffusion problem. Exact and estimated error.

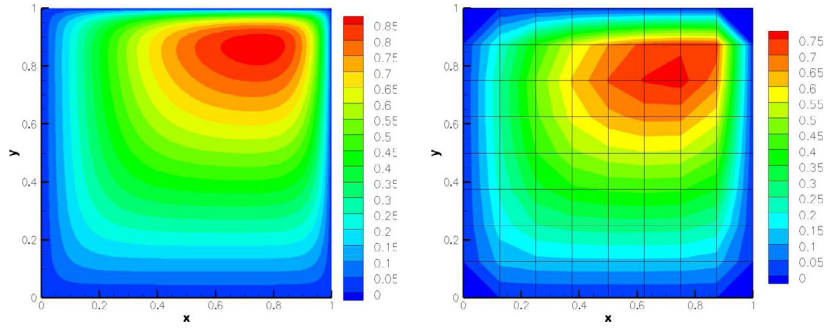

(a) Reference solution (b) FEM solution

Fig. 20. 2D Convection–diffusion equation. Reference and FEM solution.

solution, u_{ref}, has been obtained in a fine mesh (100×100 elements) and is assumed to be similar to the exact solution.

The internal residual error, u'_{bub}, is depicted in Fig. 21a using six bubble functions per element. On the other hand, the error pollution is computed solving Eq. (113). Fig. 21b shows this error term. Finally, the estimated error is the addition of both components. We can appreciate in Fig. 22 that the reference error, $u'_{\text{ref}} = u_{\text{ref}} - \bar{u}$, and the estimated error are similar. The error is mainly concentrated in the boundary layer where the solution is more abrupt.

6. Conclusion

Explicit and *implicit* a posteriori error estimators have been derived from the variational multiscale theory (VMS). The error estimators, which are based on a model that introduces approximations compatible with the theory of stabilized methods, include both, element interior and inter-element residuals. The element interior residual is key for predicting the error in the hyperbolic regime, whereas the inter-element residual, in the diffusive regime.

It has been shown that the error constants can be written in the form of *error* time scales, which have been calculated explicitly from element Green's functions. Incompressible flows require a slightly different approach, and the error time scales are precomputed from unitary problems.

Numerical examples confirm that the global efficiencies are close to one and that the local efficiencies are a good approximation of the true error, mainly in areas where the errors are large.

Thus, the proposed a posteriori error estimator leads to a very economical and robust technique for fluid problems computed with stabilized methods and can be readily implemented in existing computer codes.

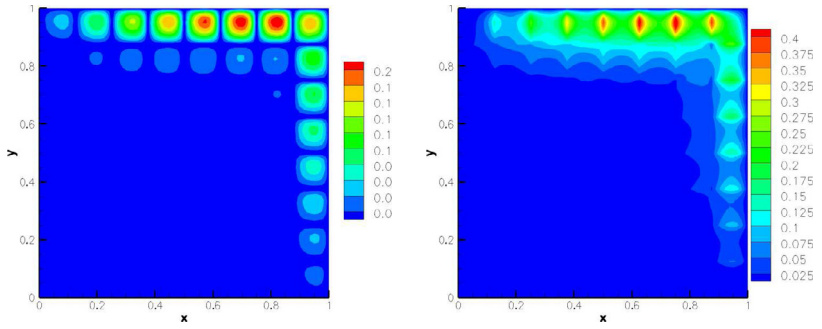

(a) u'_{bub} (b) u'_{poll}

Fig. 21. 2D Convection–diffusion equation. Internal residual error and inter-element error.

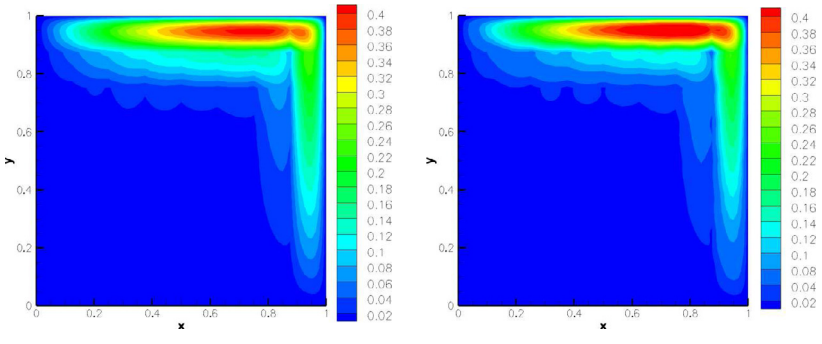

(a) Reference error (b) Estimated error

Fig. 22. 2D Convection–diffusion equation. Reference error and estimated pointwise error.

A study on the nature of the error shows that the error can be decomposed into an element interior contribution described by residual-free bubbles (or a sufficiently rich bubble space) plus an inter-element contribution, described by global free-space Green's functions. This decomposition has been applied successfully to both, Galerkin and SUPG solutions.

The success of this estimator can be explained by the fact that it solves *a-priori* the local dual problems at the element level and since the error distribution is practically local for methods stemming from H_0^1 projection, these represent fairly well the exact error. Moreover, the proposed technology achieves similar accuracy as implicit methods with less computational cost, since it is not necessary to solve any differential equation to calculate the error.

Declaration of competing interest

The authors declare that they have no known competing financial interests or personal relationships that could have appeared to influence the work reported in this paper.

Data availability

No data was used for the research described in the article.

Acknowledgments

This work has been partially funded by the Ministerio de Economía *y* Competitividad, Spain under contract PID2019-106099RB-C44 (AEI/FEDER,UE), Gobierno de Aragón/FEDER-UE, Spain (Grupo de Investigacion de Referencia de Mecanica de Fluidos Computacional T32_20R).

References

[1] T.J. Hughes, G. Scovazzi, L.P. Franca, Multiscale and stabilized methods, Encycl. Comput. Mech. Second Ed. (2018) 1–64.
[2] R. Codina, S. Badia, J. Baiges, J. Principe, Variational multiscale methods in computational fluid dynamics, Encycl. Comput. Mech. (2017) 1–28.
[3] L. Franca, G. Hauke, A. Masud, Revisiting stabilized finite element methods for the advective-diffusive equation, Comput. Methods Appl. Mech. Engrg. 195 (2006) 1560–1572.
[4] T. Hughes, Multiscale phenomena: Green's functions, the Dirichlet-to-Neumann formulation, subgrid scale models, bubbles and the origins of stabilized methods, Comput. Methods Appl. Mech. Engrg. 127 (1995) 387–401.
[5] T. Hughes, G. Feijoo, L. Mazzei, J. Quincy, The variational multiscale method: A paradigm for computational mechanics, Comput. Methods Appl. Mech. Engrg. 166 (1998) 3–24.
[6] T.J. Hughes, J.R. Stewart, A space-time formulation for multiscale phenomena, J. Comput. Appl. Math. 74 (1) (1996) 217–229.
[7] M. Ainsworth, J.T. Oden, A Posterior Error Estimation in Finite Element Analysis, John Wiley & Sons, 2000.
[8] I. Babuška, W. Rheinboldt, Analysis of optimal finite element meshes in R^1, Math. Comp. 33 (1979) 435–463.
[9] I.M. Babuška, A. Miller, A feedback finite element method with a posteriori error estimation part 1, Comput. Methods Appl. Mech. Engrg. 61 (1987) 1–40.
[10] D. Kelly, J. Gago, O. Zienkiewicz, I. Babuška, A posterior error analysis and adaptive processes in the finite element method. Part I– Error analysis, Internat. J. Numer. Methods Engrg. 19 (1983) 1593–1610.
[11] O.C. Zienkiewicz, J.Z. Zhu, A simple error estimator in the finite element method, Internat. J. Numer. Methods Engrg. 24 (1987) 337–357.
[12] O.C. Zienkiewicz, J.Z. Zhu, Adaptivity and mesh generation, Internat. J. Numer. Methods Engrg. 32 (1991) 783–810.
[13] O.C. Zienkiewicz, J.Z. Zhu, The superconvergent patch recovery and a posteriori error estimates. Part 1: The recovery technique, Internat. J. Numer. Methods Engrg. 33 (1992) 1331–1364.
[14] O.C. Zienkiewicz, J.Z. Zhu, The superconvergent patch recovery and a posteriori error estimates. Part 2: Error estimates and adaptivity, Internat. J. Numer. Methods Engrg. 33 (1992) 1365–1382.
[15] M. Ainsworth, A. Craig, A posteriori error in the finite element method, Numer. Math. 60 (1991) 429–463.
[16] J. Wu, J. Zhu, J. Smelter, O. Zienkiewicz, Error estimation and adaptivity in Navier-Stokes incompressible flows, Comput. Mech. 6 (1990) 259–271.
[17] G. Bugeda, E. Oñate, Adaptive mesh refinement techniques for aerodynamic problems, in: H. Alder, J. Heinrich, S. Lavanchy, E. Oñate, B. Suárez (Eds.), Actas Métodos numéricos en ingeniería y ciencias aplicadas, Math. Comp., 1992, pp. 513–522,
[18] E. Oñate, J. Arteaga, J. Garcia, R. Flores, Error estimation and mesh adaptivity in incompressible viscous flows using a residual power approach, Comput. Methods Appl. Mech. Engrg. 195 (2006) 339–362.
[19] I.M. Babuška, W.C. Rheinboldt, A posteriori error estimates for the finite element, Internat. J. Numer. Methods Engrg. 12 (1978) 1597–1615.
[20] I.M. Babuška, W.C. Rheinboldt, Error estimates for adaptive finite element computations, SIAM J. Numer. Anal. 18 (1978) 736–754.
[21] I. Babuška, W. Rheinboldt, Adaptive approaches and reliability estimations in finite element analysis, Comput. Methods Appl. Mech. Engrg. 17 (1979) 519–540.
[22] R. Bank, A. Weiser, Some a posteriori error estimators for elliptic partial differential equations, Math. Comp. 44 (1985) 283–301.
[23] H. Jin, S. Prudhomme, A posteriori error estimation of steady-state finite element solutions of the Navier-Stokes equations by a subdomain residual method, Comput. Methods Appl. Mech. Engrg. 159 (1998) 19–48.
[24] P. Díez, A. Huerta, A posteriori error estimation for standard finite element analysis, Comput. Methods Appl. Mech. Engrng. 163 (1998) 141–157.
[25] A. Huerta, P. Diez, Error estimation including pollution assessment for nonlinear finite element analysis, Comput. Methods Appl. Mech. Engrg. 181 (2000) 21–41.
[26] N. Parés, P. Díez, A. Huerta, Subdomain-based flux-free a posteriori error estimators, Comput. Methods Appl. Mech. Engrng. 195 (2006) 297–323.
[27] K. Eriksson, C. Johnson, An adaptive finite element method for linear elliptic problems, Comput. Methods Appl. Mech. Engrg. 50 (1988) 361–383.
[28] M. Ainsworth, J. Oden, A unified approach to a posterior error estimation using element residual methods, Numer. Math. 65 (1993) 23–50.
[29] J. Stewart, T. Hughes, An a posteriori error estimator and hp-adaptive strategy for finite element discretizations of the Helmholzt equation in exterior domains, Finite Elem. Anal. Des. 25 (1997) 1–26.
[30] J. Stewart, T. Hughes, A tutorial in elementary finite element error analysis: A systematic presentation of a priori and a posteriori error estimates, Comput. Methods Appl. Mech. Engrg. 158 (1998) 1–22.
[31] J. Oden, L. Demkowicz, W. Rachowicz, T. Westermann, A posteriori error analysis in finite elements: The element residual method for symmetrizable problems with applications to compressible Euler and Navier-Stokes equations, Comput. Methods Appl. Mech. Engrg. 82 (1990) 183–203.
[32] J. Oden, W. Wu, M. Ainsworth, An a posterior error estimate for finite element approximations of the Navier-Stokes equations, Comput. Methods Appl. Mech. Engrg. 111 (1994) 185–202.
[33] C. Johnson, Adaptive finite element methods for diffusion and convection problems, Comput. Methods Appl. Mech. Engrg. 82 (1990) 301–322.
[34] C. Johnson, Finite Element Methods for Flow Problems, Tech. Rep., 1, AGARD Report 787 (AGARD, 7 Rue Ancelle, 92299 Neuilly sur Seine, France), 1992, pp. 1–47.

[35] C. Johnson, P. Hansbo, Adaptive finite element methods in computational mechanics, Comput. Methods Appl. Mech. Engrg. 101 (1992) 143–181.
[36] T. Strouboulis, J. Oden, A posteriori error estimation of finite element approximations in fluid mechanics, Comput. Methods Appl. Mech. Engrg. 98 (1990) 201–242.
[37] R. Verfürth, A posteriori error estimators for convection-diffusion equations, Numer. Math. 80 (1998) 641–663.
[38] M. Paraschivoiu, J. Peraire, A.T. Patera, A posteriori finite element bounds for linear-functional outputs of elliptic partial differential equations, Comput. Methods Appl. Mech. Engrg. 150 (1997) 289–312.
[39] D. Venditti, D. Darmofal, Adjoint error estimation and grid adaptation for functional outputs: Application to quasi-one-dimensional flow, J. Comput. Phys. 164 (2000) 204–227.
[40] D. Venditti, D. Darmofal, Grid adaptation for functional outputs: Application to two-dimensional inviscid flows, J. Comput. Phys. 176 (2002) 40.
[41] D. Venditti, D. Darmofal, Anisotropic grid adaptation for functional outputs: application to two-dimensional viscous flows, J. Comput. Phys. 187 (2003) 22–46.
[42] K. Fidkowski, D. Darmofal, Review of output-based error estimation and mesh adaptation in computational fluid dynamics, AIAA J. 49 (2011) 673–694, http://dx.doi.org/10.2514/1.J050073.
[43] R. Verfürth, A posteriori error estimators for the Stokes problem, Numer. Math. 55 (1989) 309–325.
[44] D. Kay, D. Silvester, A posteriori error estimation for stabilized mixed approximations of the Stokes equations, SIAM J. Sci. Comput. 21 (4) (1999) 1321–1336.
[45] R.E. Bank, B.D. Welfert, A posteriori error estimates for the Stokes problem, SIAM J. Numer. Anal. 28 (3) (1991) 591–623.
[46] F. Larsson, P. Díez, A. Huerta, A flux-free a posteriori error estimator for the incompressible Stokes problem using a mixed FE formulation, Comput. Methods Appl. Mech. Engrg. 199 (37) (2010) 2383–2402.
[47] M. Ainsworth, J.T. Oden, A posterior error estimates for Stokes' and Oseen's equations, SIAM J. Numer. Anal. 34 (1997) 228–245.
[48] F. Nobile, A Posteriori Error Estimates for the Finite Element Approximation of the Stokes Problem, Tech. Rep., ICES, The University of Texas at Austin, 2003.
[49] A. Russo, A posteriori error estimators for the Stokes problem, Appl. Math. Lett. 8 (2) (1995) 1–4.
[50] L. Song, Y. Hou, H. Zheng, Adaptive variational multiscale method for the Stokes equations, Internat. J. Numer. Methods Fluids 71 (11) (2013) 1369–1381.
[51] J. Hoffman, C. Johnson, Adaptive finite element methods for incompressible fluid flow, in: T. Barth, H. Deconinck (Eds.), Error Estimation and Adaptive Discretization Methods in Computational Fluid Dynamics, in: Lecture Notes in Computational Science and Engineering, vol. 25, Springer, 2002, pp. 97–158.
[52] J.T. Oden, W. Wu, M. Ainsworth, An a posteriori error estimate for finite element approximations of the Navier-Stokes equations, Comput. Methods Appl. Mech. Engrg. 111 (1–2) (1994) 185–202.
[53] S. Berrone, Adaptive discretization of stationary and incompressible Navier–Stokes equations by stabilized finite element methods, Comput. Methods Appl. Mech. Engrg. 190 (34) (2001) 4435–4455.
[54] E. Berrone, Robustness in a posteriori error analysis for FEM flow models, Numer. Math. 91 (2002) 389–422.
[55] K. Eriksson, D. Estep, P. Hansbo, C. Johnson, Introduction to adaptive methods for differential equations, Acta Numer. 105 (1995) 105–158.
[56] R. Verfürth, A Review of a Posteriori Error Estimation and Adaptive Mesh-Refinement Techniques, Wiley-Teuber, 1996.
[57] W. Bangerth, R. Rannacher, Adaptive Finite Element Methods for Differential Equations, Birkhäuser, 2003.
[58] V. John, A numerical study of a posteriori error estimators for convection-diffusion equations, Comput. Methods Appl. Mech. Engrg. 190 (2000) 757–781.
[59] A. Papastavrou, R. Verfürth, A posteriori error estimators for stationary convection-diffusion problems: a computational comparison, Comput. Methods Appl. Mech. Engrg. 189 (2000) 449–462.
[60] V. John, J. Novo, A robust SUPG norm a posteriori error estimator for stationary convection–diffusion equations, Comput. Methods Appl. Mech. Engrg. 255 (2013) 289–305.
[61] V. John, P. Knobloch, J. Novo, Finite elements for scalar convection-dominated equations and incompressible flow problems: a never ending story? Comput. Vis. Sci. 19 (2018) 47–63.
[62] R. Reyes, R. Codina, Element boundary terms in reduced order models for flow problems: Domain decomposition and adaptive coarse mesh hyper-reduction, Comput. Methods Appl. Mech. Engrg. (ISSN: 0045-7825) 368 (2020) 113159, http://dx.doi.org/10.1016/j.cma.2020.113159, URL https://www.sciencedirect.com/science/article/pii/S0045782520303443.
[63] R. Codina, R. Reyes, J. Baiges, A posteriori error estimates in a finite element VMS-based reduced order model for the incompressible Navier-Stokes equations, Mech. Res. Commun. (ISSN: 0093-6413) 112 (2021) 103599, http://dx.doi.org/10.1016/j.mechrescom.2020.103599, URL https://www.sciencedirect.com/science/article/pii/S0093641320301270, Special issue honoring G.I. Taylor Medalist Prof. Arif Masud.
[64] A. Masud, G. Scovazzi, A heterogeneous multiscale modeling framework for hierarchical systems of partial differential equations, Internat. J. Numer. Methods Fluids 65 (1–3) (2011) 28–42, http://dx.doi.org/10.1002/fld.2456, URL https://onlinelibrary.wiley.com/doi/abs/10.1002/fld.2456.
[65] O. Colomes, G. Scovazzi, J. Guilleminot, On the robustness of variational multiscale error estimators for the forward propagation of uncertainty, Comput. Methods Appl. Mech. Engrg. 342 (2018) 384–413.
[66] M. Scott, D. Thomas, E. Evans, Isogeometric spline forests, Comput. Methods Appl. Mech. Engrg. (ISSN: 0045-7825) 269 (2014) 222–264, http://dx.doi.org/10.1016/j.cma.2013.10.024, URL https://www.sciencedirect.com/science/article/pii/S0045782513002764.

[67] E. Evans, M. Scott, X. Li, D. Thomas, Hierarchical T-splines: Analysis-suitability, Bézier extraction, and application as an adaptive basis for isogeometric analysis, Comput. Methods Appl. Mech. Engrg. (ISSN: 0045-7825) 284 (2015) 1–20, http://dx.doi.org/10.1016/j.cma.2014.05.019, URL https://www.sciencedirect.com/science/article/pii/S0045782514001807, Isogeometric Analysis Special Issue.
[68] V.V. Garg, R.H. Stogner, Local enhancement of functional evaluation and adjoint error estimation for variational multiscale formulations, Comput. Methods Appl. Mech. Engrg. (ISSN: 0045-7825) 354 (2019) 119–142, http://dx.doi.org/10.1016/j.cma.2019.05.023, URL https://www.sciencedirect.com/science/article/pii/S0045782519302932.
[69] T. Hughes, The Finite Element Method:Linear Static and Dynamic Finite Element Analysis, Dover Publications, 2000.
[70] T. Hughes, G. Sangalli, Variational multiscale analysis: the fine-scale Green's function, projection, optimization, localization and stabilized methods, SIAM J. Numer. Anal. 45 (2) (2007) 539–557.
[71] F. Cirak, E. Ramm, A posteriori error estimation and adaptivity for linear elasticity using the reciprocal theorem, Comput. Methods Appl. Mech. Engrg. 156 (1–4) (1998) 351–362.
[72] T. Grätsch, F. Hartmann, Pointwise error estimation and adaptivity for the finite element method using fundamental solutions, Comput. Mech. 37 (5) (2006) 394–407.
[73] F. Hartmann, Green's Functions and Finite Elements, Springer, 2013.
[74] D. Estep, M. Holst, M. Larson, Generalized Green's functions and the effective domain of influence, Commun. Numer. Meth. Engrg. 18 (2002) 15–30.
[75] G. Hauke, D. Fuster, M.H. Doweidar, Variational multiscale a-posteriori error estimation for the multi-dimensional transport equation, Comput. Methods Appl. Mech. Engrg. 197 (2008) 2701–2718.
[76] G. Hauke, M.H. Doweidar, D. Fuster, A posteriori error estimation for computational fluid dynamics. The variational multiscale approach, in: E. Ramm, R. de Borst (Eds.), Multiscale Methods in Computational Mechanics, in: Lecture Notes in Applied and Computational Mechanics, vol. 55, Springer, 2010, pp. 19–38.
[77] G. Hauke, M.H. Doweidar, M. Miana, The multiscale approach to error estimation and adaptivity, Comput. Methods Appl. Mech. Engrg. 195 (2006) 1573–1593.
[78] G. Hauke, M.H. Doweidar, M. Miana, Proper intrinsic scales for a-posteriori multiscale error estimation, Comput. Methods Appl. Mech. Engrg. 195 (2006) 3983–4001.
[79] G. Hauke, M.H. Doweidar, Intrinsic scales and a posteriori multiscale error estimation for piecewise-linear functions and residuals, Int. J. Comput. Fluid Dyn. 20 (2006) 211–222.
[80] S. Brenner, L. Scott, The Mathematical Theory of Finite Element Methods, Springer-Verlag, 2002.
[81] M.G. Larson, A. Målqvist, Adaptive variational multiscale methods based on a posteriori error estimation: Energy norm estimates for elliptic problems, Comput. Methods Appl. Mech. Engrg. 196 (2007) 2313–2324.
[82] F. Brezzi, M. Bristeau, L.P. Franca, M. Mallet, G. Rogé, A relationship between stabilized finite element methods and the Galerkin method with bubble functions, Comput. Methods Appl. Mech. Engrg. 96 (1992) 117–129.
[83] F. Brezzi, A. Russo, Choosing bubbles for advection-diffusion problems, Math. Models Methods Appl. Sci. 4 (1994) 571–587.
[84] F. Brezzi, L. Franca, T. Hughes, A. Russo, $b = \int g$, Comput. Methods Appl. Mech. Engrg. 145 (1997) 329–339.
[85] A.N. Agarwal, P. Pinsky, Stabilized element residual method (SERM): A posteriori error estimation for the advection-diffusion equation, J. Comput. Appl. Math. 74 (1996) 3–17.
[86] A. Russo, A posteriori error estimators via bubble functions, Math. Models Methods Appl. Sci. 1 (1996) 33–41.
[87] A. Masud, T. Truster, Modeling of steep layers in singularly perturbed diffusion-reaction equation via flexible fine-scale basis, Comput. Methods Appl. Mech. Engrg. 372 (2020) 113343.
[88] G. Hauke, M.H. Doweidar, D. Fuster, A. Gomez, J. Sayas, Application of variational a-posteriori multiscale error estimation to higher-order elements, Comput. Mech. 38 (2006) 382–389.
[89] D. Estep, M. Holst, D. Mikulencak, Accounting for stability: a posteriori error estimates based on residuals and variational analysis, Commun. Numer. Meth. Engrg. 18 (2002) 15–30.
[90] L. Franca, S. Frey, T. Hughes, Stabilized finite element methods: I. Application to the advective-diffusive model, Comput. Methods Appl. Mech. Engrg. 95 (1992) 253–276.
[91] L. Franca, F. Valentin, On an improved unusual stabilized finite element method for the advective-reactive-diffusive equation, Comput. Methods Appl. Mech. Engrg. 190 (2000) 1785–1800.
[92] G. Hauke, A simple stabilized method for the advection-diffusion-reaction equation, Comput. Methods Appl. Mech. Engrg. 191 (2002) 2925–2947.
[93] I. Harari, L. Franca, S. Oliveira, Streamline design of stability parameters for advection-diffusion problems, J. Comput. Phys. 171 (2001) 115–131.
[94] R. Courant, D. Hilbert, Methods of Mathematical Physics, Vol. I, John Wiley & Sons, 1989.
[95] T.C. Rebollo, B.M. Dia, A variational multi-scale method with spectral approximation of the sub-scales: Application to the 1D advection–diffusion equations, Comput. Methods Appl. Mech. Engrg. 285 (2015) 406–426.
[96] T.C. Rebollo, S. Fernandez-Garcia, On the computation of the stabilized coefficients for the 1D spectral VMS method, SEMA 75 (2018) 573–590.
[97] T. Chacón Rebollo, S. Fernández-García, M. Gómez-Mármol, Anisotropic VMS solution of advection–diffusion problems by spectral approximation of sub-grid scales, J. Comput. Appl. Math. 380 (2020) 112959.
[98] T.C. Rebollo, S. Fernández-García, D. Moreno-Lopez, I.S. Muñoz, Spectral variational multi-scale method for parabolic problems: application to 1D transient advection-diffusion equations, Comput. Appl. Math. 42 (1) (2023) 43.
[99] G. Hauke, M.H. Doweidar, S. Fuentes, Mesh adaptivity for the transport equation led by variational multiscale error estimators, Internat. J. Numer. Methods Fluids 69 (2012) 1835–1850.

[100] G. Hauke, D. Fuster, Variational multiscale a-posteriori error estimation for quantities of interest, J. Appl. Mech. 76 (2009) 021201, 1–6.
[101] B.N. Granzow, M.S. Shephard, A.A. Oberai, Output-based error estimation and mesh adaptation for variational multiscale methods, Comput. Methods Appl. Mech. Engrg. 322 (2017) 441–459.
[102] M.G. Larson, A. Målqvist, Adaptive variational multiscale methods based on a posteriori error estimation: Duality techniques for elliptic problems, Comput. Sci. Eng. 44 (2005) 181–193.
[103] M.G. Larson, A. Målqvist, An adaptive variational multiscale method for convection-diffusion problems, Commun. Numer. Methods. Eng. 25 (2009) 65–79.
[104] A. ElSheik, S. Chidiac, W. Smith, A posteriori error estimation based on numerical realization of the variational multiscale method, Comput. Methods Appl. Mech. Engrg. 197 (2008) 3637–3656.
[105] A. ElSheik, S. Smith, S. Chidiac, Numerical investigation of the reliability of a posteriori error estimation for advection-diffusion equations, Commun. Numer. Methods. Eng. 24 (2008) 711–726.
[106] R. Araya, F. Valentin, A multiscale a posteriori error estimate, Comput. Methods Appl. Mech. Engrg. 194 (2005) 2077–2094.
[107] R. Araya, E. Behrens, R. Rodriguez, An adaptive stabilized finite element scheme for the advection-reaction-diffusion equation, Appl. Numer. Math. 54 (2005) 491–503.
[108] R. Araya, E. Behrens, R. Rodriguez, Error estimator advection-reaction-diffusion equations based on solution of local problems, Appl. Numer. Math. 206 (2007) 440–453.
[109] A. Bazile, E. Hachem, J. Larroya-Huguet, Y. Mesri, Variational multiscale error estimator for anisotropic adaptive fluid mechanic simulations: Application to convection-diffusion problems, Comput. Methods Appl. Mech. Engrg. 331 (2018) 94–115.
[110] A. Jha, A residual based a posteriori error estimators for AFC schemes for convection-diffusion equations, Comput. Math. Appl. (ISSN: 0898-1221) 97 (2021) 86–99, http://dx.doi.org/10.1016/j.camwa.2021.05.031, URL https://www.sciencedirect.com/science/article/pii/S0898122121002236.
[111] G. Hauke, D. Fuster, F. Lizarraga, Variational multiscale a posteriori error estimation for systems: The Euler and Navier–Stokes equations, Comput. Methods Appl. Mech. Engrg. 283 (2015) 1493–1524.
[112] G. Hauke, T. Hughes, A unified approach to compressible and incompressible flows, Comput. Methods Appl. Mech. Engrg. 113 (1994) 389–395.
[113] G. Hauke, T. Hughes, A comparative study of different sets of variables for solving compressible and incompressible flows, Comput. Methods Appl. Mech. Engrg. 153 (1998) 1–44.
[114] C. Bayona-Roa, R. Codina, J. Baiges, Variational multiscale error estimators for the adaptive mesh refinement of compressible flow simulations, Comput. Methods Appl. Mech. Engrg. 337 (2018) 501–526.
[115] G. Hauke, J. Lanzarote, Simulation of low-speed buoyant flows with a stabilized compressible/incompressible formulation: The full Navier-Stokes approach versus the Boussinesq model, Algorithms 15 (8) (2022) 278.
[116] S. Tendulkar, F. Yang, R. Nastasia, M.W. Beall, A.A. Oberai, M.S. Shephard, O. Sahni, Geometry and adaptive mesh update procedures for ballistics simulations, in: R. Sevilla, S. Perotto, K. Morgan (Eds.), Mesh Generation and Adaptation: Cutting-Edge Techniques, Springer International Publishing, Cham, ISBN: 978-3-030-92540-6, 2022, pp. 209–231.
[117] F. Yang, A. Chandra, Y. Zhang, S. Tendulkar, R. Nastasia, A.A. Oberai, M.S. Shephard, O. Sahni, A parallel interface tracking approach for evolving geometry problems, Eng. Comput. 38 (5) (2022) 4289–4305, http://dx.doi.org/10.1007/s00366-021-01386-8,
[118] M. Polner, L. Pesch, J. van der Vegt, Construction of stabilization operators for Galerkin least-squares discretizations of compressible and incompressible flows, Comput. Methods Appl. Mech. Engrg. 196 (2007) 2431–2448.
[119] D. Irisarri, G. Hauke, A posteriori error estimation and adaptivity based on VMS for the Stokes problem, Internat. J. Numer. Methods Fluids 88 (10–11) (2018) 493–520.
[120] D. Irisarri, G. Hauke, A posteriori error estimation and adaptivity based on VMS for the incompressible Navier-Stokes equations, Comput. Methods Appl. Mech. Engrg. 373 (2021) 113508.
[121] T.J. Hughes, L.P. Franca, A new finite element formulation for computational fluid dynamics: VII. The Stokes problem with various well-posed boundary conditions: symmetric formulations that converge for all velocity/pressure spaces, Comput. Methods Appl. Mech. Engrg. 65 (1) (1987) 85–96.
[122] J. Donea, A. Huerta, Finite Element Methods for Flow Problems, Wiley, 2003.
[123] I. Babuška, The finite element method with Lagrangian multipliers, Numer. Math. 20 (3) (1973) 179–192.
[124] F. Brezzi, On the existence, uniqueness and approximation of saddle-point problems arising from Lagrangian multipliers, Revue Française d'Automatique Inf. Recherche Oper. Anal. Numer. 8 (2) (1974) 129–151.
[125] F. Brezzi, J. Pitkäranta, On the Stabilization of Finite Element Approximations of the Stokes Equations, Springer, 1984.
[126] R. Pierre, Simple C0 approximations for the computation of incompressible flows, Comput. Methods Appl. Mech. Engrg. 68 (2) (1988) 205–227.
[127] N. Kechkar, D. Silvester, Analysis of locally stabilized mixed finite element methods for the Stokes problem, Math. Comp. 58 (197) (1992) 1–10.
[128] L.P. Franca, T.J. Hughes, R. Stenberg, Stabilized finite element methods for the Stokes problem, Incompressible Comput. Fluid Dyn. (1993) 87–107.
[129] L. Franca, A. Russo, Approximation of the Stokes problem by residual-free macro bubbles, East-West J. Numer. Math. 4 (1996) 265–278.
[130] M. Behr, T. Tezduyar, Finite element solution strategies for large-scale flow simulations, Comput. Methods Appl. Mech. Engrg. 112 (1–4) (1994) 3–24.
[131] R. Codina, Stabilization of incompressibility and convection through orthogonal sub-scales in finite element methods, Comput. Methods Appl. Mech. Engrg. 190 (13) (2000) 1579–1599.

[132] W. Dettmer, D. Peric, An analysis of the time integration algorithms for the finite element solutions of incompressible Navier-Stokes equations based on a stabilised formulation, Comput. Methods Appl. Mech. Engrg. 192 (9) (2003) 1177–1226.
[133] A. Masud, R. Khurram, A multiscale/stabilized finite element method for the incompressible Navier-Stokes equations, Comput. Methods Appl. Mech. Engrg. 195 (2006) 1750–1777.
[134] L. Franca, S. Frey, Stabilized finite element methods: II. The incompressible Navier-Stokes equations, Comput. Methods Appl. Mech. Engrg. 99 (1992) 209–233.
[135] Y. Bazilevs, V. Calo, J. Cottrell, T. Hughes, A. Reali, G. Scovazzi, Variational multiscale residual-based turbulence modeling for large eddy simulation of incompressible flows, Comput. Methods Appl. Mech. Engrg. 197 (1) (2007) 173–201.
[136] D. Irisarri, G. Hauke, A posteriori pointwise error computation for 2-D transport equations based on the variational multiscale method, Comput. Methods Appl. Mech. Engrg. 311 (2016) 648–670.
[137] D. Irisarri, G. Hauke, Pointwise error estimation for the one-dimensional transport equation based on the variational multiscale method, Int. J. Comput. Methods 14 (4) (2017) 30, http://dx.doi.org/10.1142/S0219876217500402, URL http://www.worldscientific.com/doi/abs/10.1142/S0219876217500402.
[138] R. Rossi, J. Cotela, N. Lafontaine, P. Dadvand, S. Idelsohn, Parallel adaptive mesh refinement for incompressible flow problems, Comput. & Fluids 80 (2013) 342–355.
[139] Y. Mesri, A. Bazile, J. Larroya-Huguet, E. Hachem, Parallel and adaptive VMS finite elements formulation for aerothermal problems, Comput. & Fluids 173 (2018) 42–50.
[140] D. Irisarri, G. Hauke, Variational multiscale a posteriori error estimation for 2nd and 4th-order ODEs, Int. J. Numer. Anal. Model. 12 (3) (2015) 430–454.
[141] A. Masud, T. Truster, L. Bergman, A variational multiscale a posteriori error estimation method for mixed form of nearly incompressible elasticity, Comput. Methods Appl. Mech. Engrg. 200 (2011) 3453–3481.
[142] G. Hauke, D. Irisarri, Variational multiscale a posteriori error estimation for systems. application to linear elasticity, Comput. Methods Appl. Mech. Engrg. 285 (2015) 291–314.
[143] J. Baiges, R. Codina, Variational multiscale error estimators for solid mechanics adaptive simulations: An Orthogonal Subgrid Scale approach, Comput. Methods Appl. Mech. Engrg. 325 (2017) 37–55.
[144] C. Carstensen, R. Verfürth, Edge residuals dominate a posteriori error estimates for low order finite element methods, SIAM J. Numer. Anal. 36 (5) (1999) 1571–1587.
[145] H. Zheng, Y. Hou, F. Shi, Adaptive variational multiscale methods for incompressible flow based on two local Gauss integrations, J. Comput. Phys. 229 (19) (2010) 7030–7041.
[146] R. Araya, R. Rebolledo, F. Valentin, On a multiscale a posteriori error estimator for the stokes and Brinkman equations, IMA J. Numer. Anal. (ISSN: 0272-4979) 41 (1) (2019) 344–380, http://dx.doi.org/10.1093/imanum/drz053.
[147] O. Colomes, G. Scovazzi, I. Sraj, O. Knio, O. Le Maître, A finite volume error estimator inspired by the variational multiscale approach, in: 2018 AIAA Non-Deterministic Approaches Conference, 2018, p. 1178.
[148] A. Bazile, Y. Mesri, J.-C. Larroya-Huguet, E. Hachem, Aerothermal impingement jet flow simulations using anisotropic multiscale mesh adaptation, in: 2018 Fluid Dynamics Conference, American Institute of Aeronautics and Astronautic, 2018, http://dx.doi.org/10.2514/6.2018-2898.
[149] J. Cotela-Dalmau, R. Rossi, A. Larese, Simulation of two- and three-dimensional viscoplastic flows using adaptive mesh refinement, Internat. J. Numer. Methods Engrg. 112 (11) (2017) 1636–1658, http://dx.doi.org/10.1002/nme.5574, URL https://onlinelibrary.wiley.com/doi/abs/10.1002/nme.5574.
[150] A. Masud, T.J. Truster, L.A. Bergman, A unified formulation for interface coupling and frictional contact modeling with embedded error estimation, Internat. J. Numer. Methods Engrg. 92 (2) (2012) 141–177.
[151] A. Masud, T.J. Truster, A framework for residual-based stabilization of incompressible finite elasticity: stabilized formulations and methods for linear triangles and tetrahedra, Comput. Methods Appl. Mech. Engrg. 267 (2013) 359–399.